

Capturing Context-Aware Route Choice Semantics for Trajectory Representation Learning

Ji Cao[†], Yu Wang[†], Tongya Zheng, Jie Song, Qinghong Guo, Zujie Ren*,
Canghong Jin, Gang Chen, Mingli Song

Abstract—Trajectory representation learning (TRL) aims to encode raw trajectory data into low-dimensional embeddings for downstream tasks such as travel time estimation, mobility prediction, and trajectory similarity analysis. From a behavioral perspective, a trajectory reflects a sequence of route choices within an urban environment. However, most existing TRL methods ignore this underlying decision-making process and instead treat trajectories as static, passive spatiotemporal sequences, thereby limiting the semantic richness of the learned representations. To bridge this gap, we propose CORE, a TRL framework that integrates context-aware route choice semantics into trajectory embeddings. CORE first incorporates a multi-granular Environment Perception Module, which leverages large language models (LLMs) to distill environmental semantics from point of interest (POI) distributions, thereby constructing a context-enriched road network. Building upon this backbone, CORE employs a Route Choice Encoder with a mixture-of-experts (MoE) architecture, which captures route choice patterns by jointly leveraging the context-enriched road network and navigational factors. Finally, a Transformer encoder aggregates the route-choice-aware representations into a global trajectory embedding. Extensive experiments on 4 real-world datasets across 6 downstream tasks demonstrate that CORE consistently outperforms 12 state-of-the-art TRL methods, achieving an average improvement of 9.79% over the best-performing baseline. Our code is available at <https://github.com/caoji2001/CORE>.

Index Terms—Trajectory representation learning, Trajectory data mining, Trajectory analysis.

I. INTRODUCTION

THE proliferation of GPS-enabled devices facilitates the large-scale collection of spatiotemporal trajectories, which record detailed movement patterns of vehicles [1], [2], [3]. These trajectories encode rich spatiotemporal semantics that support a wide range of downstream applications, including travel time estimation [4], mobility prediction [5], and trajectory similarity analysis [6].

Ji Cao, Yu Wang, Gang Chen, and Mingli Song are with the College of Computer Science and Technology, Zhejiang University, Hangzhou 310027, China; Ji Cao is also with the Zhejiang Lab, Hangzhou 311121, China (e-mail: {caoj25, yu.wang, cg, brooksong}@zju.edu.cn).

Tongya Zheng and Canghong Jin are with the Zhejiang Provincial Engineering Research Center for Real-Time SmartTech in Urban Security Governance, Hangzhou City University, Hangzhou 310015, China (e-mail: doujiang_zheng@163.com; jinch@hzcu.edu.cn).

Jie Song is with the School of Software Technology, Zhejiang University, Ningbo 315100, China (e-mail: sjie@zju.edu.cn).

Qinghong Guo is with the Polytechnic Institute of Zhejiang University, Hangzhou 310015, China (e-mail: q.h_guo@zju.edu.cn).

Zujie Ren is with the Zhejiang Lab, Hangzhou 311121, China (e-mail: zujie.rzj@zhejianglab.com).

[†] Ji Cao and Yu Wang contributed equally to this work.

* Zujie Ren is the corresponding author.



Fig. 1. Even with the same OD pair, different drivers may choose substantially different routes, reflecting complex route choice behaviors.

Trajectory representation learning (TRL), which encodes raw trajectory data into low-dimensional embeddings, receives considerable attention for its ability to extract informative spatiotemporal patterns [7], [8], [9]. Early TRL methods [10], [11] primarily employ LSTMs [12] or GRUs [13] as sequence backbones. For example, Trembr [10] uses an RNN-based encoder-decoder to reconstruct trajectories, thereby capturing their spatiotemporal characteristics. Motivated by the strong sequence-modeling capability of the Transformer architecture [14], recent studies [7], [9], [15] increasingly adopt it as the backbone. For instance, START [9] integrates a graph attention network (GAT) [16] with a time-aware Transformer encoder to capture travel semantics and temporal regularities, whereas GREEN [17] leverages a Transformer architecture to jointly model road- and grid-level trajectories. Despite these advances, most existing TRL methods still treat trajectories as static, passive spatiotemporal sequences, neglecting the underlying behavioral mechanisms that govern trajectory formation.

In reality, a trajectory is the outcome of a sequence of route choices, which are intrinsically contextualized by the surrounding urban environment [18], [19]. As illustrated in Figure 1, three trajectories share the same origin–destination (OD) pair: the blue trajectory follows urban expressways with light traffic (passing a park and a stadium), like prioritizing efficiency and minimal congestion; the red trajectory also uses expressways but experiences moderate traffic (passing an exhibition center and a park), reflecting a trade-off between travel time and the views along the route; in contrast, the green trajectory partially diverts into a heavily congested residential area, indicating a stopover or a preference for familiar roads. These divergences result from a sequence of

latent route choices within the urban context. Consequently, modeling trajectories solely as static, passive spatiotemporal sequences, while ignoring the underlying route choices, produces representations with limited behavioral fidelity, which in turn hinders performance on downstream tasks.

However, capturing route choice semantics from trajectory data involves two closely interrelated challenges: (1) **External Urban Context Perception**: Route choices essentially manifest as sequences of decisions within an urban environment. Consequently, accurately characterizing such behavioral patterns necessitates a precise perception of the environmental context. (2) **Internal Route Choice Complexity**: Route choice logic varies substantially across different intersection contexts, which makes it non-trivial for a unified model to capture such heterogeneous behavioral patterns.

To address these challenges, we propose **CORE**, a framework for capturing **C**ontext-aware **R**oute choice **E** semantics for effective trajectory representation learning. CORE treats trajectories as sequences of context-aware route choices and consists of two key components. First, to achieve context awareness, we develop a multi-granular Environment Perception Module. This module leverages the world knowledge encoded in large language models (LLMs) to distill environmental semantics from point of interest (POI) distributions at both road-segment and urban-functional levels, yielding a context-aware road network that serves as a semantic backbone. Second, to capture the latent route choices governing observed trajectories, we introduce a Route Choice Encoder. It integrates the aforementioned context-aware road network with navigational factors, and employs a mixture-of-experts (MoE) [20] architecture to capture heterogeneous routing semantics across diverse intersection contexts. A Transformer encoder then aggregates the resulting route-choice-aware representations into a global trajectory embedding. The entire framework is end-to-end trainable and utilizes a contrastive learning objective [21] for pretraining.

To evaluate CORE, we conduct extensive experiments on 4 real-world trajectory datasets across 6 downstream tasks. The results demonstrate that CORE consistently outperforms 12 *state-of-the-art* TRL methods, achieving an average performance improvement of 9.79% over the best-performing baseline. In addition, an ablation study shows that each module of CORE contributes to performance, while further analysis confirms that CORE exhibits superior data efficiency in few-shot scenarios and competitive computational efficiency.

To summarize, we make the following three contributions:

- We identify a critical oversight in existing TRL methods: trajectories are treated as simple sequences of road segments, rather than as sequences of route choices within an urban environment, and this fundamentally limits these models’ ability to capture the intrinsic decision-making semantics embedded in trajectories.
- We propose CORE as a more effective TRL framework. CORE learns trajectory embeddings by incorporating context-aware route choice semantics as an inductive bias, using a multi-granular Environment Perception Module, an MoE-based Route Choice Encoder, and a Transformer-based aggregation layer.

- We conduct extensive experiments on 4 real-world trajectory datasets to evaluate CORE, and compare it with 12 *state-of-the-art* baselines. The results show that CORE consistently outperforms existing TRL methods.

II. RELATED WORK

A. Trajectory Representation Learning

TRL aims to map raw trajectory data into low-dimensional embeddings that can be leveraged by a wide range of spatiotemporal analysis tasks. Early TRL methods predominantly learn task-specific trajectory embeddings. For example, t2vec [22], NEUTRAJ [23], and GTS [24] are specifically designed for trajectory similarity computation, whereas DeepTTE [25], WDR [26], and ConSTGAT [27] primarily focus on travel time estimation. However, such task-specific representations often exhibit limited generalization ability across downstream tasks. To overcome this limitation, subsequent research shifts toward general-purpose pretraining, aiming to learn versatile, task-agnostic trajectory representations that are effective across a wide range of downstream applications. For instance, Trembr [10] and RED [28] employ sequence-to-sequence models [13] to reconstruct trajectories, while JGRM [29] adopts a masked language modeling (MLM) objective [30] to capture intrinsic spatiotemporal characteristics within trajectories. Inspired by the success of contrastive learning in computer vision [21], a series of subsequent studies introduce contrastive objectives into TRL: PIM [11] maximizes mutual information between global and local views of trajectories, JCLRNT [7] aligns trajectory and road network features through cross-scale contrastive learning, and START [9] performs contrastive learning across trajectories to capture travel semantics and temporal regularities. More recent efforts extend the contrastive learning idea to multi-view or multimodal settings: GREEN [17] aligns complementary grid-based and road-level trajectory representations using a contrastive loss, and TRACK [31] bridges trajectory data with traffic states to obtain traffic-aware embeddings. Nevertheless, existing TRL approaches still model trajectories as generic spatiotemporal sequences, largely overlooking the underlying route choices that reflect travelers’ decision-making processes.

B. Road Network Representation Learning

Road network representation learning aims to learn latent representations of road segments or intersections in an urban network. Early methods such as IRN2Vec [32] and SRN2Vec [33] extend node2vec [34] by incorporating spatial locality and mobility patterns to obtain road network representations. Building on this line of work, Toast [15] jointly models traffic patterns and mobility semantics to enhance embedding robustness, while DyToast [35] further introduces a unified temporal encoding to learn time-aware representations. Given the strong capability of graph neural networks (GNNs) [36] in modeling non-Euclidean structures, subsequent studies primarily adopt GNN-based architectures. For example, RFN [37] utilizes a graph convolutional network (GCN) [38] to model road segments and intersections jointly. HRNR [39] constructs a three-level hierarchical GNN to

learn road network embeddings that integrate both structural and functional properties, and HyperRoad [40] leverages hypergraphs [41] to capture higher-order relationships among multiple road segments across regions. SARN [42] further integrates graph contrastive learning (GCL) [43] to strengthen spatial modeling and improve representation robustness. However, the incorporation of rich urban environmental semantics into road network embeddings remains underexplored. To address this limitation, we leverage LLMs to distill human-centric semantics from multi-granular POI distributions and inject these semantics into road network embeddings, thereby yielding context-aware road network representations.

C. LLMs for Spatiotemporal Modeling

Driven by the progress of LLMs in natural language processing [44], recent work explores their potential in spatiotemporal data mining. In mobility modeling, LLMob [45], CoPB [46], and AgentMove [47] formulate mobility generation as an LLM-based planning problem, where agents reason over individual routines and urban context to synthesize daily activities. For POI recommendation, Mobility-LLM [48], LLM4POI [49], and POI-Enhancer [50] convert user check-in sequences and POI attributes into natural language descriptions and, through prompt engineering, inject LLM knowledge into spatiotemporal encodings to better capture user intent and preferences, thereby improving next-POI prediction. In traffic forecasting, PromptST [51], UrbanGPT [52], and UniST [53] adopt LLM paradigms such as pretraining and instruction tuning to build general-purpose spatiotemporal predictors.

To the best of our knowledge, the studies most closely related to our Environment Perception Module are TrajCogn [54] and POI-Enhancer [50]. However, TrajCogn mainly leverages LLMs at the trajectory level by embedding POI names into a textual prompt, and POI-Enhancer focuses on POI-level semantic enhancement by using LLMs to enrich individual POI representations. Both lines largely treat POIs as isolated semantic units and fail to explicitly ground such environmental semantics onto the underlying road network structure. In contrast, CORE uses LLMs to derive multi-granular environmental semantics from POI distributions and injects them into road network embeddings, thereby bridging heterogeneous POI and road network data on a unified context-aware road network that supports subsequent route choice encoding.

III. PRELIMINARIES

A. Definitions

Definition 1 (GPS Trajectory). A GPS trajectory is defined as a sequence of points $\mathcal{T}^{GPS} = \{\tau_1^{GPS}, \tau_2^{GPS}, \dots, \tau_n^{GPS}\}$, where each $\tau_i^{GPS} = (lat_i, lon_i, t_i)$ consists of the latitude, longitude, and timestamp, respectively.

Definition 2 (Road Network). A road network is represented as a directed graph $\mathcal{G} = \langle \mathcal{V}, \mathcal{E} \rangle$, where \mathcal{V} is the set of road segments and $\mathcal{E} \subseteq \mathcal{V} \times \mathcal{V}$ denotes the set of directed edges capturing their connectivity. A directed edge $e_{i,j} \in \mathcal{E}$ indicates that segment v_j is directly reachable from segment v_i .

Definition 3 (Road Network Constrained Trajectory). A road network constrained trajectory¹ $\mathcal{T} = \{\tau_1, \tau_2, \dots, \tau_n\}$ is defined as a timestamped sequence of road segments obtained by map matching a raw GPS trajectory to the underlying road network. Each element $\tau_i = (r_i, t_i)$ consists of a road segment ID r_i and its associated timestamp t_i .

Definition 4 (Point of Interest). A point of interest (POI) is formalized as a geospatial entity tuple $\mathbf{p} = (\text{latitude}, \text{longitude}, \text{category}, \text{subcategory}, \text{name})$, where latitude and longitude denote the geographic coordinates, category and subcategory define a two-level functional taxonomy (e.g., category “Shopping Services” and subcategory “Convenience Stores”), and name specifies the entity’s proper name (e.g., “7-Eleven”).

B. Problem Statement

Given a trajectory dataset $\mathcal{D} = \{\mathcal{T}_1, \mathcal{T}_2, \dots, \mathcal{T}_{|\mathcal{D}|}\}$, our objective is to learn an encoding function:

$$F : \mathcal{T} \rightarrow \mathbf{z} \in \mathbb{R}^d, \quad (1)$$

which maps a trajectory \mathcal{T} to a d -dimensional representation \mathbf{z} . We expect the mapping function $F(\cdot)$ to exhibit the following two core capabilities: (1) **Spatiotemporal Pattern Capture:** effective encoding of the intrinsic spatiotemporal patterns of trajectories into a low-dimensional representation space. (2) **Task Versatility:** flexible adaptation to diverse downstream applications, such as destination prediction, travel time estimation, and similar trajectory retrieval.

IV. METHODOLOGY

In this section, we introduce CORE, a TRL framework that treats trajectories as observable traces of sequential route choice decisions. As illustrated in Figure 2, CORE comprises two key components: (1) an Environment Perception Module, which constructs a context-aware road network from multi-granular POI distributions; and (2) a Route Choice Encoder, which models route choices by integrating the context-aware road network with navigational factors via an MoE architecture. Finally, a Transformer encoder aggregates these sequential behavioral representations into a global trajectory embedding. The entire framework is end-to-end trainable and is pretrained with a contrastive learning objective.

A. Environment Perception Module

To effectively model route choices, it is essential to capture the underlying environmental semantics that constitute the decision-making context. Although transportation network semantics are jointly shaped by intrinsic network attributes and the surrounding urban context (e.g., land use, commercial vitality) [55], the latter is often difficult to quantify directly. Because POIs provide a rich characterization of urban functions, we use them as observable proxies for environmental semantics and design a multi-granular modeling scheme: a fine-grained level that characterizes road-segment-level context, and a coarse-grained level that quantifies the influence

¹For convenience, “trajectory” will refer to a “road network constrained trajectory” in unambiguous contexts throughout this paper.

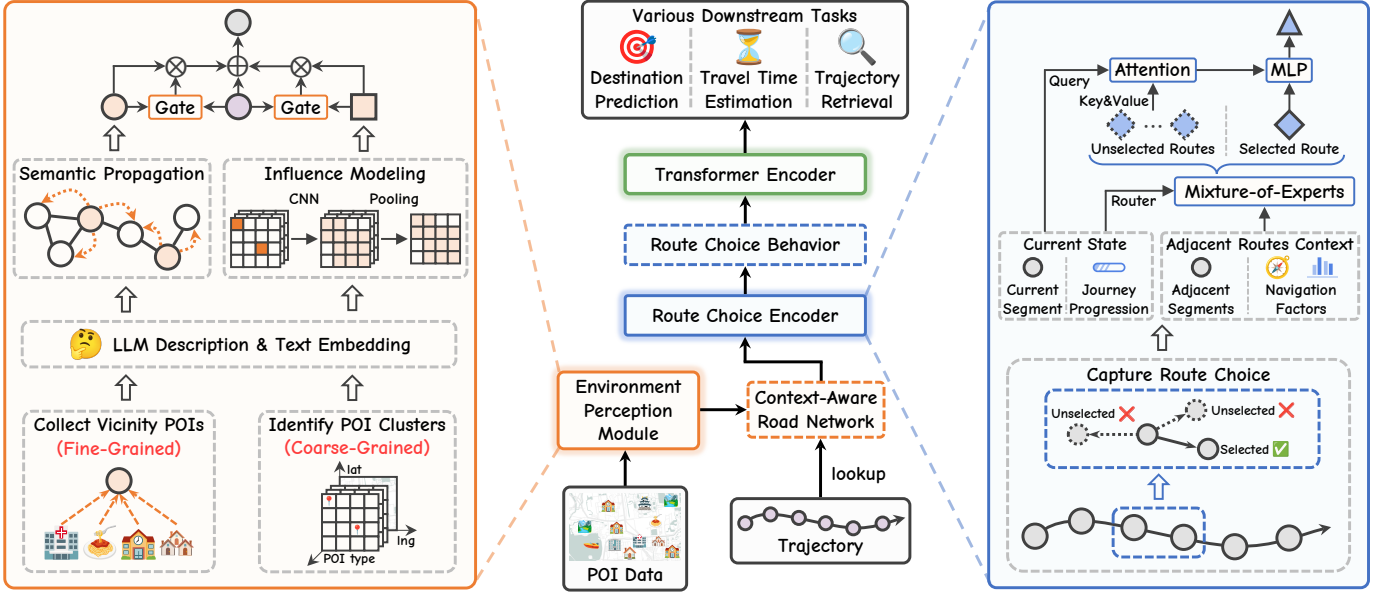


Fig. 2. Overview of CORE. The Environment Perception Module first constructs a context-aware road network based on the environmental semantics implied by POI distributions. Building on this backbone, the Route Choice Encoder models route choices by jointly leveraging the context-enriched road network and navigational factors. A Transformer encoder finally aggregates the resulting route-choice-aware representations into global trajectory embeddings.

of the broader urban functional structure. Together, these two levels yield a context-aware road network representation that serves as the backbone for subsequent route choice encoding.

1) *Fine-Grained Semantic Modeling*: At the fine-grained level, we characterize the local urban context of each road segment by aggregating POIs within a radius δ (set to $\delta = 100$ m in our experiments). However, bridging the semantic gap between heterogeneous POI attributes and latent urban functions remains non-trivial; naive aggregation of POI categories fails to capture the emergent semantics arising from their spatial co-occurrence (e.g., reasoning that a cluster of cafes, bookstores, and galleries signifies an artistic and cultural district). To bridge this gap, we leverage the extensive world knowledge embedded in LLMs to interpret POI distributions. Specifically, we employ Qwen3-8B [56] to distill high-level textual descriptions from raw POI sequences, which are subsequently encoded by Qwen3-Embedding-8B [57] into dense environmental vectors $\mathbf{e}_i^{\text{fine}} \in \mathbb{R}^d$ (please refer to Appendix A-A for prompt templates and illustrative examples).

Nevertheless, applying LLM-based descriptions to every road segment in a large-scale network is computationally prohibitive. For instance, the main urban area of Beijing contains approximately 40,000 road segments, and segment-wise processing leads to severe scalability issues. Fortunately, as shown in Figure 3, visitation is strongly long-tailed: a small set of *critical segments* carries the majority of traffic, while most segments are only sparsely visited.

Motivated by these observations, we design an efficient semantic representation scheme. Specifically, we select the top 20% of segments with the highest traffic volume as *critical segments*, while the remaining infrequently visited segments are initialized to zero (i.e., $\mathbf{e}_i^{\text{fine}} = \mathbf{0}$), and we reconstruct their semantics via a three-layer GAT with $\mathbf{h}_i^{(0)} = \mathbf{e}_i^{\text{fine}}$. The feature

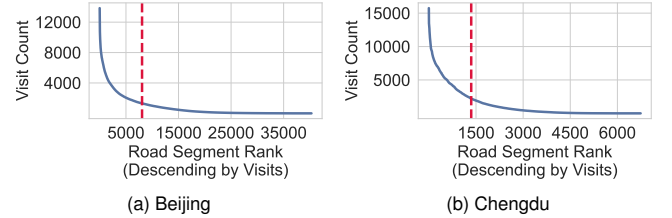


Fig. 3. Visit count distributions over road segments in Beijing and Chengdu. Segments to the left of the red dashed line are the top 20% most visited.

propagation and aggregation at each layer $\ell \in \{0, 1, 2\}$ is:

$$\mathbf{h}_i^{(\ell+1)} = \sigma \left(\sum_{j \in \mathcal{N}(i) \cup \{i\}} \alpha_{ij}^{(\ell)} \mathbf{W}^{(\ell)} \mathbf{h}_j^{(\ell)} \right), \quad (2)$$

where the attention coefficient $\alpha_{ij}^{(\ell)}$ is computed as:

$$\alpha_{ij}^{(\ell)} = \frac{\exp \left(\sigma \left(\mathbf{a}^{(\ell)\top} [\mathbf{W}^{(\ell)} \mathbf{h}_i^{(\ell)} \parallel \mathbf{W}^{(\ell)} \mathbf{h}_j^{(\ell)}] \right) \right)}{\sum_{k \in \mathcal{N}(i) \cup \{i\}} \exp \left(\sigma \left(\mathbf{a}^{(\ell)\top} [\mathbf{W}^{(\ell)} \mathbf{h}_i^{(\ell)} \parallel \mathbf{W}^{(\ell)} \mathbf{h}_k^{(\ell)}] \right) \right)}. \quad (3)$$

Here, $\mathcal{N}(i)$ is the set of neighboring road segments of i , $\mathbf{a}^{(\ell)} \in \mathbb{R}^{2d}$ and $\mathbf{W}^{(\ell)} \in \mathbb{R}^{d \times d}$ are learnable parameters, and σ is a non-linear activation function. The choice of the 20% selection ratio is empirically validated in Section V-F1, which demonstrates that this sparse initialization strategy achieves performance nearly identical to full-coverage LLM reasoning (covering 100% of segments), while effectively reducing computational overhead. After three layers, the propagation expands the semantic coverage from the initial 20% to the majority of the road network, yielding a final representation $\tilde{\mathbf{e}}_i^{\text{fine}} = \mathbf{h}_i^{(3)}$ enriched with local environmental context. For the remaining uncovered segments, valid representations are

still effectively characterized by the subsequent coarse-grained semantics and basic road attributes.

2) *Coarse-Grained Semantic Modeling*: While fine-grained semantic modeling captures local environmental attributes at the level of individual road segments, it does not fully characterize each segment’s role within the city’s broader functional structure, which in turn shapes route choice behavior. To address this limitation, we introduce coarse-grained environmental semantic modeling, which encodes the urban functional structure and complements the fine-grained features.

Given that urban functions (e.g., commercial, residential) are unevenly distributed and exhibit spatial clustering [58], [59], we model these concentrations as *functional hotspots* to characterize the urban functional structure. Let the urban domain be $\Omega = [0, W) \times [0, H)$ with horizontal and vertical extents W and H . Then the (i, j) -th grid is defined as:

$$g_{(i,j)} = [(i-1)L, \min\{iL, W\}) \times [(j-1)L, \min\{jL, H\}), \quad (4)$$

for $i = 1, \dots, \lceil \frac{W}{L} \rceil$ and $j = 1, \dots, \lceil \frac{H}{L} \rceil$, where L is the grid side length (set to 1000 m). Subsequently, for each POI category c , we quantify the POI density within each grid and identify *functional hotspots* \mathcal{H}_c as the top 10% of grids with the highest counts. For any hotspot grid $g_{(i,j)}$ of category c , we follow the fine-grained semantic pipeline: the grid’s category- c POI set is summarized with Qwen3-8B [56] and the generated text is embedded by Qwen3-Embedding-8B [57] to obtain a d -dimensional vector (prompt templates and illustrative examples in Appendix A-B). Grids that are not hotspots are assigned the zero vector. Formally, we define:

$$\mathbf{e}_{(i,j),c}^{\text{coarse}} = \begin{cases} \mathcal{F}(\{\mathbf{p} \mid \mathbf{p} \text{ in } g_{(i,j)}, \mathbf{p}.\text{category} = c\}), & g_{(i,j)} \in \mathcal{H}_c \\ \mathbf{0}, & g_{(i,j)} \notin \mathcal{H}_c \end{cases} \quad (5)$$

where $\mathcal{F}(\cdot)$ denotes the composition of an LLM-based description step followed by a text embedding encoder.

To capture spillover effects, in which *functional hotspots* influence adjacent grids (e.g., commercial centers substantially influence the spatiotemporal patterns of surrounding traffic), we apply a 3×3 convolution kernel to the feature maps of each POI category c :

$$\tilde{\mathbf{e}}_{(i,j),c}^{\text{coarse}} = \sum_{a=-1}^1 \sum_{b=-1}^1 \mathbf{W}_{(a,b)} \mathbf{e}_{(i+a,j+b),c}^{\text{coarse}}, \quad (6)$$

with learnable weights $\mathbf{W}_{(a,b)} \in \mathbb{R}^{d \times d}$ for each relative position (a, b) , and zero-padding applied at grid boundaries.

Finally, we perform average pooling along the POI category dimension within each grid, yielding $\tilde{\mathbf{e}}_{(i,j)}^{\text{coarse}}$ as the representation of grid (i, j) .

3) *Multi-Granular Semantic Fusion*: To construct a unified, context-aware representation of urban road networks, we integrate the aforementioned multi-granular environmental semantics with basic segment attributes, where the attribute vector $\mathbf{r}_i \in \mathbb{R}^d$ for segment i is the element-wise sum of the embeddings of road type, length, in-degree, and out-degree:

$$\mathbf{r}_i = \mathbf{r}_i^{\text{type}} + \mathbf{r}_i^{\text{length}} + \mathbf{r}_i^{\text{in}} + \mathbf{r}_i^{\text{out}}. \quad (7)$$

We then fuse these attributes with the fine- and coarse-grained environmental semantics through a gating mechanism, yielding the final context-aware road segment representation $\tilde{\mathbf{r}}_i$:

$$\tilde{\mathbf{r}}_i = \mathbf{r}_i + \tilde{\mathbf{e}}_i^{\text{fine}} \odot \text{Gate}(\tilde{\mathbf{e}}_i^{\text{fine}} \parallel \mathbf{r}_i) + \tilde{\mathbf{e}}_{\text{grid}(i)}^{\text{coarse}} \odot \text{Gate}(\tilde{\mathbf{e}}_{\text{grid}(i)}^{\text{coarse}} \parallel \mathbf{r}_i). \quad (8)$$

Here, $\text{grid}(\cdot)$ maps a road segment to its corresponding grid, and the gating function is defined as:

$$\text{Gate}(\mathbf{x}) = \tanh(\mathbf{W}_{\text{Gate}}\mathbf{x} + \mathbf{b}_{\text{Gate}}), \quad (9)$$

where $\mathbf{W}_{\text{Gate}} \in \mathbb{R}^{d \times 2d}$, $\mathbf{b}_{\text{Gate}} \in \mathbb{R}^d$ are learnable parameters.

B. Route Choice Encoder

Building on the context-aware road network, the Route Choice Encoder is designed to characterize the sequential route choice process within trajectories. Given a trajectory as a sequence of road segments (r_1, \dots, r_n) , each decision step i selects the next segment r_{i+1} from the adjacent set $\mathcal{N}(r_i)$. We represent this step using two feature groups: a *current state* $\mathbf{s}_{\text{current}} \in \mathbb{R}^{2d}$ and an *adjacent route context* $\mathbf{s}_{r_c} \in \mathbb{R}^{3d}$:

- **Current State.** For the current segment r_i , let $\tilde{\mathbf{r}}_{r_i} \in \mathbb{R}^d$ be its context-aware representation. We augment it with a *journey progression* scalar $\rho_i \in [0, 1]$ to obtain:

$$\mathbf{s}_{\text{current}} = \tilde{\mathbf{r}}_{r_i} \parallel \mathbf{w}_\rho \rho_i, \quad (10)$$

where $\mathbf{w}_\rho \in \mathbb{R}^d$ is a learnable vector, and

$$\rho_i = \frac{\sum_{j=1}^i r_j.\text{length}}{\sum_{j=1}^n r_j.\text{length}} \in [0, 1]. \quad (11)$$

- **Adjacent Route Context.** For each candidate $r_c \in \mathcal{N}(r_i)$, let $\tilde{\mathbf{r}}_{r_c} \in \mathbb{R}^d$ be its context-aware representation. We further encode two navigational factors: the *historical transition likelihood* $P(r_c \mid r_i)$ and the *destination-oriented directional deviation* $\Delta\theta_{r_c}$, forming:

$$\mathbf{s}_{r_c} = \tilde{\mathbf{r}}_{r_c} \parallel \mathbf{w}_P P(r_c \mid r_i) \parallel \mathbf{w}_\Delta \Delta\theta_{r_c}, \quad (12)$$

where $\mathbf{w}_P, \mathbf{w}_\Delta \in \mathbb{R}^d$ are learnable parameters. The transition likelihood $P(r_c \mid r_i)$ is computed from historical counts $N(r_i \rightarrow r_c)$ over the adjacency set:

$$P(r_c \mid r_i) = \frac{N(r_i \rightarrow r_c)}{\sum_{r'_c \in \mathcal{N}(r_i)} N(r_i \rightarrow r'_c)}. \quad (13)$$

The directional deviation $\Delta\theta_{r_c}$ measures how much turning toward r_c deviates from the direct bearing to the destination segment r_n :

$$\Delta\theta_{r_c} = \angle(\overrightarrow{r_i r'_c}, \overrightarrow{r_i r_n}). \quad (14)$$

Given the substantial variability in route choice logic across different intersections (e.g., highway interchanges vs. multi-functional commercial streets), we employ DeepSeekMoE [20] to capture these complex patterns. Specifically, the *current state* $\mathbf{s}_{\text{current}}$ is fed to the MoE router, which dynamically selects an expert ensemble tailored to the current route choice context. Subsequently, the MoE model transforms the *adjacent*

route context \mathbf{s}_{r_c} for all candidates $r_c \in \mathcal{N}(r_i)$, yielding contextual representations $\tilde{\mathbf{s}}_{r_c}$ by the expert networks:

$$\tilde{\mathbf{s}}_{r_c} = \text{FFN}(\mathbf{s}_{r_c}) + \sum_{i=1}^{n_e} (g_i \text{FFN}_i(\mathbf{s}_{r_c})), \quad (15)$$

$$g_i = \begin{cases} s_i, & s_i \in \text{Top-k}(\{s_j \mid 1 \leq j \leq n_e\}, k) \\ 0, & \text{otherwise} \end{cases}, \quad (16)$$

$$s_i = \text{Softmax}(\mathbf{s}_{\text{current}} \mathbf{w}_i^T), \quad (17)$$

where n_e denotes the number of experts and k is the number of activated experts (in our implementation, we set $n_e = 8$ and $k = 2$). $\text{FFN}(\cdot)$ is a shared feed-forward network, and $\text{FFN}_i(\cdot)$ is the i -th expert network, both yielding d -dimensional outputs. $\mathbf{w}_i \in \mathbb{R}^{2d}$ denotes the router’s learnable weight vector for the i -th expert.

Subsequently, to capture route choice semantics, we compute the behavior representation at r_i by synthesizing information from both the *selected* segment and its *unselected* counterparts. Specifically, we treat the next segment r_{i+1} as *selected*, while the remaining adjacent segments $\mathcal{N}(r_i) \setminus \{r_{i+1}\}$ are regarded as *unselected* (for the terminal segment r_n , all adjacent segments $\mathcal{N}(r_n)$ are considered *unselected*). To aggregate the representations of all unselected segments, we employ an attention mechanism:

$$\tilde{\mathbf{s}}_{\mathcal{N}(r_i) \setminus \{r_{i+1}\}} = \sum_{r \in \mathcal{N}(r_i) \setminus \{r_{i+1}\}} \alpha_r \tilde{\mathbf{s}}_r \mathbf{W}_v, \quad (18)$$

$$\alpha_r = \text{Softmax}((\mathbf{W}_q \mathbf{s}_{\text{current}})(\mathbf{W}_k \tilde{\mathbf{s}}_r)^T / \sqrt{d}), \quad (19)$$

where $\mathbf{W}_q \in \mathbb{R}^{d \times 2d}$, $\mathbf{W}_k, \mathbf{W}_v \in \mathbb{R}^{d \times d}$ are learnable parameters for query, key, and value, respectively. Finally, we encode the decision logic by concatenating the representation of the *selected* segment $\tilde{\mathbf{s}}_{r_{i+1}}$ with the aggregated *unselected* context $\tilde{\mathbf{s}}_{\mathcal{N}(r_i) \setminus \{r_{i+1}\}}$ (if the unselected set is empty, $\tilde{\mathbf{s}}_{\mathcal{N}(r_i) \setminus \{r_{i+1}\}}$ is represented by a zero vector), and feeding them into an MLP to obtain the route choice behavior representation \mathbf{o}_i :

$$\mathbf{o}_i = \text{MLP}(\tilde{\mathbf{s}}_{r_{i+1}} \parallel \tilde{\mathbf{s}}_{\mathcal{N}(r_i) \setminus \{r_{i+1}\}}). \quad (20)$$

C. Trajectory Embedding and Pretraining

To obtain a global trajectory embedding, we first enrich the route choice behavior representation \mathbf{o}_i for each spatiotemporal point (r_i, t_i) with time-of-day and day-of-week context before sequence aggregation:

$$\mathbf{x}_i = \mathbf{o}_i + \mathbf{t}_{m(t_i)}^m + \mathbf{t}_{d(t_i)}^d. \quad (21)$$

Here, $\mathbf{t}_{m(t_i)}^m$ and $\mathbf{t}_{d(t_i)}^d$ are learnable embeddings for minute-of-day (1 to 1440) and day-of-week (1 to 7) of the timestamp t_i . We then prepend a learnable classification token [CLS] and pass the sequence to a Transformer encoder [14]:

$$(\mathbf{z}, \tilde{\mathbf{x}}_1, \dots, \tilde{\mathbf{x}}_n) = \text{TransformerEncoder}([\text{CLS}], \mathbf{x}_1, \dots, \mathbf{x}_n), \quad (22)$$

where \mathbf{z} serves as the global trajectory embedding.

Following prior TRL studies [9], [31], we then adopt a contrastive learning objective for pretraining to learn robust and discriminative representations. Specifically, we utilize the following two data augmentation strategies:

- **Trajectory Cropping.** To effectively capture spatial characteristics, we randomly crop the start or end of a trajectory. The crop ratio is sampled from $U(0.05, 0.15)$.
- **Temporal Perturbation.** To enhance temporal modeling, we perturb travel times for 15% of the segments: for a segment with Δt , set $\Delta t' = \Delta t - r(\Delta t - \Delta t_{\text{avg}})$, where Δt_{avg} is the segment-wise average and $r \sim U(0.15, 0.30)$.

Subsequently, for each trajectory in a batch \mathcal{B} , we apply both augmentations to obtain $2|\mathcal{B}|$ views and optimize with the NT-Xent loss [21], which promotes agreement between positive pairs while separating them from negatives:

$$\mathcal{L} = -\frac{1}{2|\mathcal{B}|} \sum_{i=1}^{2|\mathcal{B}|} \left[\log \frac{\exp(\text{sim}(\mathbf{z}_i, \mathbf{z}_{\text{pos}(i)})/\tau)}{\sum_{j=1}^{2|\mathcal{B}|} \mathbb{1}_{[j \neq i]} \exp(\text{sim}(\mathbf{z}_i, \mathbf{z}_j)/\tau)} \right], \quad (23)$$

where $\text{sim}(\cdot, \cdot)$ denotes cosine similarity, $\tau = 0.07$ is the temperature, and $\text{pos}(i)$ is the positive sample index for \mathbf{z}_i .

V. EXPERIMENTS

To assess the effectiveness of the CORE framework, we conduct comprehensive experiments on four real-world trajectory datasets and seek to answer the following research questions:

- **RQ1:** How does CORE compare with state-of-the-art TRL methods on downstream tasks?
- **RQ2:** How does each module in CORE contribute to the overall model performance?
- **RQ3:** How efficient is CORE in terms of data utilization and computational costs?
- **RQ4:** What insights do qualitative visualizations provide into the representations learned by CORE?
- **RQ5:** How sensitive is CORE to hyperparameters, the choice of LLM backbone, and POI data completeness?

A. Experimental Setup

1) *Datasets:* We evaluate CORE across four real-world trajectory datasets: Beijing, Chengdu, Xi’an, and Porto. The corresponding road networks are extracted from OpenStreetMap² using OSMnx [60], and all trajectories are map-matched with FMM [61]. Each trajectory dataset is chronologically partitioned into training, validation, and test sets in a 7:1:2 ratio. The dataset statistics are summarized in Table I, and their spatial distributions are visualized in Figure 4.

TABLE I
STATISTICS OF THE FOUR REAL-WORLD TRAJECTORY DATASETS.

Dataset	# Trajectories	# Segments	Avg. Length	Avg. Time
Beijing	1,010,325	40,306	6.60 km	15.57 min
Chengdu	431,581	6741	4.10 km	8.77 min
Xi’an	407,181	6795	4.54 km	11.59 min
Porto	695,085	11,095	4.08 km	8.02 min

In addition, we collect POI data for Beijing, Chengdu, and Xi’an using the Amap API³. For Porto, where the Amap API is unavailable due to geographic restrictions, we obtain POI data from OpenStreetMap via the Overpass API⁴. The statistics of the POI data are reported in Table II.

²<https://www.openstreetmap.org>

³<https://lbs.amap.com>

⁴<https://overpass-api.de>

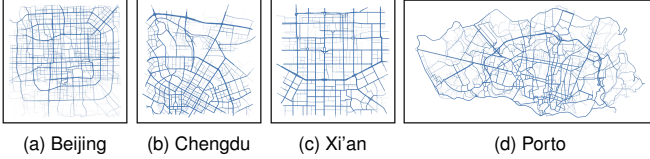


Fig. 4. Spatial distributions of the four trajectory datasets.

TABLE II
STATISTICS OF THE POI DATA.

Dataset	# POIs	# Categories	# Subcategories
Beijing	706,115	14	128
Chengdu	141,918	14	126
Xi'an	87,309	14	124
Porto	8652	22	264

2) *Baselines*: We compare CORE against the following 12 *state-of-the-art* baselines, including 9 general-purpose TRL methods and 3 trajectory generation models (TS-TrajGen, STEGA, and HOSER):

- **HRNR** [39] employs a hierarchical GNN to jointly model both structural and functional properties of road networks.
- **Toast** [15] combines a context-aware skip-gram module for modeling traffic patterns with a trajectory-enhanced Transformer for capturing travel semantics.
- **PIM** [11] employs mutual information maximization to learn trajectory representations.
- **DyToast** [35] extends Toast [15] by employing trigonometric functions to better capture temporal patterns.
- **JCLRNT** [7] jointly learns road network and trajectory representations via contrastive learning.
- **START** [9] employs GAT to encode road representations enriched with travel semantics, and Transformer [14] to capture periodic temporal regularities.
- **TS-TrajGen** [62] generates trajectories by combining a two-stage GAN with the A* search algorithm.
- **STEGA** [63] performs traffic trajectory generation via semantic-aware graph learning.
- **JGRM** [29] jointly encodes GPS and road trajectories using a Transformer-based architecture, and is pretrained with self-supervised objectives.
- **HOSER** [64] holistically fuses semantics from multi-level road networks, multi-granular trajectories, and destination information for trajectory generation.
- **TRACK** [31] bridges traffic states and trajectory data to jointly learn dynamic representations.
- **GREEN** [17] employs CNN and GNN encoders for grid- and road-level features, respectively, and fuses them via cross-attention to construct trajectory embeddings.

3) *Implementation Details*: All experiments are conducted on a single NVIDIA RTX A6000 GPU. For a fair comparison, all baselines use the same embedding dimension as CORE ($d = 128$) and the same Transformer depth (6 layers). Road segment embeddings are computed via Equation (7). For pretraining and fine-tuning, all TRL methods are trained for 50 epochs using the AdamW [65] optimizer with a batch size of

TABLE III
EVALUATION ON ROAD LABEL PREDICTION TASK.

Methods	Beijing		Chengdu	
	Macro-F1↑	Micro-F1↑	Macro-F1↑	Micro-F1↑
HRNR	0.7912	0.7990	0.7054	0.7903
Toast	0.5868	0.6285	0.4200	0.7508
PIM	0.6284	0.6519	0.4684	0.7569
DyToast	0.6263	0.6488	0.4511	0.7548
JCLRNT	0.6479	0.6751	0.6376	0.7754
START	0.7574	0.7776	0.6535	0.7805
JGRM	0.7822	0.7903	0.6819	0.7892
TRACK	0.6744	0.6948	0.6107	0.7590
GREEN	0.6705	0.7006	0.6182	0.7692
CORE	0.9303	0.9408	0.8574	0.9009
Improvement(%)	17.58	17.75	21.55	13.99

Methods	Xi'an		Porto	
	Macro-F1↑	Micro-F1↑	Macro-F1↑	Micro-F1↑
HRNR	0.6459	0.6651	0.6408	0.7172
Toast	0.4308	0.5129	0.3779	0.6380
PIM	0.4357	0.5155	0.4207	0.6056
DyToast	0.4327	0.5149	0.4315	0.6267
JCLRNT	0.4582	0.5076	0.4936	0.6312
START	0.6225	0.6363	0.6136	0.6900
JGRM	0.6376	0.6355	0.6322	0.7086
TRACK	0.4652	0.5190	0.5493	0.6607
GREEN	0.5290	0.5545	0.5799	0.6833
CORE	0.8456	0.8367	0.8073	0.8551
Improvement(%)	30.92	25.80	25.98	19.23

64. The learning rate is initialized to 2×10^{-4} , linearly warmed up over the first 5 epochs, and then cosine-decayed to 1×10^{-6} . All reported results are averaged over five independent trials to ensure statistical reliability. For CORE's MoE-based Route Choice Encoder, we employ Loss-Free Balancing [66] to achieve load balancing among experts.

B. Overall Performance (RQ1)

We evaluate the learned representations on six downstream tasks: *road label prediction* (RLP), *destination prediction* (DP), *travel time estimation* (TTE), *similar trajectory retrieval* (STR), *path ranking* (PR), and *trajectory generation* (TG). These tasks assess our model's capabilities at two distinct levels: RLP evaluates intermediate road segment representations, whereas the other five evaluate final trajectory-level representations. For STR, similarity is computed directly from learned trajectory embeddings, whereas for the remaining tasks (RLP, DP, TTE, PR, and TG), we attach a task-specific MLP head and fine-tune the model end-to-end.

1) *Road Label Prediction*: Following prior work [7], [35], we evaluate the learned road segment representations by predicting the number of lanes, an attribute withheld from the inputs in Equation (7). The task is optimized using cross-entropy loss and is evaluated using Macro-F1 and Micro-F1. The results in Table III indicate that CORE achieves the best performance across all four datasets, primarily due to its Environment Perception Module, which captures real-world environmental semantics. Furthermore, HRNR [39] performs well among all baseline methods, primarily benefiting from its hierarchical road network modeling that can reflect the underlying structure of urban space.

2) *Travel Time Estimation*: This task aims to predict the time a vehicle needs to complete a given path. We formulate it

TABLE IV
EVALUATION ON TRAVEL TIME ESTIMATION TASK.

Methods	Beijing			Chengdu		
	MAE↓	RMSE↓	MAPE↓	MAE↓	RMSE↓	MAPE↓
HRNR	5.1072	9.4108	0.3388	1.7796	2.7743	0.2308
Toast	5.1042	9.2255	0.3423	1.7804	2.7730	0.2301
PIM	5.1622	9.3977	0.3456	1.7877	2.7778	0.2292
DyToast	4.2883	8.3221	0.2863	1.5071	2.3719	0.2025
JCLRNT	5.0191	9.1380	0.3281	1.7959	2.7878	0.2343
START	5.0103	9.1894	0.3376	1.4901	2.3406	0.2010
JGRM	4.4038	8.5129	0.2954	1.4523	2.3005	0.1899
TRACK	<u>4.0375</u>	<u>8.0509</u>	<u>0.2773</u>	1.4307	2.2401	<u>0.1864</u>
GREEN	4.1657	8.2444	0.2915	<u>1.4259</u>	<u>2.2245</u>	0.1882
CORE	3.6703	6.9956	0.2551	1.3681	2.1719	0.1801
Improvement(%)	9.09	13.11	8.01	4.05	2.36	3.38

Methods	Xi'an			Porto		
	MAE↓	RMSE↓	MAPE↓	MAE↓	RMSE↓	MAPE↓
HRNR	2.9449	4.7241	0.2835	1.5942	2.3751	0.2504
Toast	2.9350	4.6983	0.2824	1.6225	2.4240	0.2541
PIM	2.9540	4.7358	0.2786	1.6647	2.4892	0.2587
DyToast	2.2856	3.7257	0.2282	1.4581	2.2460	0.2406
JCLRNT	2.9791	4.7513	0.2869	1.6093	2.4102	0.2544
START	2.3700	3.7994	0.2482	1.6077	2.4095	0.2536
JGRM	2.3021	3.8054	0.2291	1.4238	2.2529	0.2270
TRACK	2.2514	<u>3.5998</u>	<u>0.2047</u>	<u>1.4001</u>	<u>2.1877</u>	<u>0.2247</u>
GREEN	2.2743	3.7211	0.2056	1.4056	2.1930	0.2283
CORE	2.1498	3.5783	0.1951	1.3519	2.1151	0.2198
Improvement(%)	4.51	0.60	4.69	3.44	3.32	2.18

TABLE V
EVALUATION ON SIMILAR TRAJECTORY RETRIEVAL TASK.

Methods	Beijing			Chengdu		
	HR@1↑	HR@5↑	MRR↑	HR@1↑	HR@5↑	MRR↑
HRNR	0.8653	0.9226	0.8914	0.6069	0.7705	0.6782
Toast	0.8532	0.9112	0.8792	0.5739	0.7180	0.6100
PIM	0.8060	0.8615	0.8323	0.5498	0.7012	0.6025
DyToast	0.8773	0.9259	0.8998	0.6256	0.7811	0.6962
JCLRNT	0.8985	0.9369	0.9166	0.7521	0.8706	0.8069
START	0.9056	<u>0.9442</u>	<u>0.9231</u>	0.7859	0.8911	0.8337
JGRM	0.8991	0.9412	0.9190	0.7903	0.9006	0.8357
TRACK	0.8941	0.9387	0.9158	0.7712	0.8831	0.8221
GREEN	<u>0.9078</u>	0.9437	0.9207	<u>0.7992</u>	<u>0.9044</u>	<u>0.8394</u>
CORE	0.9611	0.9911	0.9729	0.9402	0.9746	0.9554
Improvement(%)	5.87	4.97	5.39	17.64	7.76	13.82

Methods	Xi'an			Porto		
	HR@1↑	HR@5↑	MRR↑	HR@1↑	HR@5↑	MRR↑
HRNR	0.6641	0.8062	0.7251	0.7856	0.9128	0.8423
Toast	0.6618	0.7838	0.6902	0.6520	0.8342	0.7280
PIM	0.6188	0.7453	0.6685	0.6437	0.8165	0.7221
DyToast	0.6900	0.8187	0.7488	0.7528	0.8874	0.8138
JCLRNT	0.8092	0.8895	0.8451	0.8064	0.9135	0.8405
START	0.8645	0.9214	0.8724	0.8153	0.9197	0.8459
JGRM	0.8699	0.9280	0.8859	0.8104	0.9154	0.8420
TRACK	0.8613	0.9255	0.8793	0.8122	0.9178	0.8446
GREEN	<u>0.8862</u>	<u>0.9403</u>	<u>0.9123</u>	<u>0.8501</u>	<u>0.9398</u>	<u>0.9145</u>
CORE	0.9540	0.9858	0.9685	0.9746	0.9930	0.9820
Improvement(%)	7.65	4.84	6.16	14.65	5.66	7.38

as a regression problem and optimize with mean squared error (MSE) loss, and we quantify the target travel time in minutes. We input only the departure time to avoid potential leakage. We report mean absolute error (MAE), root mean square error (RMSE), and mean absolute percentage error (MAPE) for evaluation. The results in Table IV show that CORE achieves the best performance, attributable to its multi-granular urban semantic perception and route choice encoding.

3) *Similar Trajectory Retrieval*: Following prior work [7], we sample two disjoint trajectory subsets from the test set, denoted \mathcal{Q} and \mathcal{D} . For each trajectory in \mathcal{Q} , we apply a detour method to construct a corresponding perturbed trajectory in \mathcal{Q}' , ensuring high trajectory-level similarity between \mathcal{Q} and

TABLE VI
EVALUATION ON DESTINATION PREDICTION TASK.

Methods	Beijing			Chengdu		
	Acc@1↑	Acc@5↑	Acc@10↑	Acc@1↑	Acc@5↑	Acc@10↑
HRNR	0.0789	0.2019	0.2613	<u>0.4168</u>	0.6215	0.6995
Toast	0.0694	0.1809	0.2374	0.3954	0.5940	0.6667
PIM	0.0629	0.1614	0.2100	0.4073	0.6129	0.6858
DyToast	0.0772	0.1846	0.2415	0.4007	0.6019	0.6703
JCLRNT	0.0782	0.1879	0.2538	0.4072	0.6154	0.6932
START	0.0856	0.2153	0.2876	0.4128	0.6231	0.7033
JGRM	0.0865	0.2180	0.2905	0.4150	0.6261	0.7044
TRACK	0.0873	0.2198	0.2939	0.4159	<u>0.6267</u>	0.7041
GREEN	<u>0.0913</u>	<u>0.2285</u>	<u>0.3062</u>	0.4060	0.6137	0.6933
CORE	0.1076	0.2647	0.3499	0.4296	0.6411	0.7189
Improvement(%)	17.85	15.84	14.27	3.07	2.30	2.06

Methods	Xi'an			Porto		
	Acc@1↑	Acc@5↑	Acc@10↑	Acc@1↑	Acc@5↑	Acc@10↑
HRNR	0.3511	0.5800	0.6624	<u>0.1659</u>	0.3624	0.4540
Toast	0.3260	0.5421	0.6247	0.1490	0.3366	0.4214
PIM	0.3396	0.5629	0.6440	0.1378	0.3190	0.4002
DyToast	0.3304	0.5451	0.6222	0.1557	0.3367	0.4254
JCLRNT	0.3430	0.5687	0.6566	0.1558	0.3508	0.4450
START	0.3499	0.5844	0.6742	0.1627	0.3649	0.4598
JGRM	0.3512	0.5834	0.6721	0.1620	0.3644	0.4593
TRACK	0.3503	0.5824	0.6705	0.1608	0.3631	0.4582
GREEN	<u>0.3550</u>	<u>0.5889</u>	<u>0.6773</u>	0.1650	<u>0.3693</u>	<u>0.4630</u>
CORE	0.3631	0.5977	0.6845	0.1734	0.3750	0.4694
Improvement(%)	2.28	1.49	1.06	4.52	1.54	1.38

TABLE VII
EVALUATION ON PATH RANKING TASK.

Methods	Beijing			Chengdu		
	τ ↑	ρ ↑	MAE↓	τ ↑	ρ ↑	MAE↓
HRNR	0.6259	0.6749	0.1492	0.7489	0.7885	0.1007
Toast	0.6298	0.6808	0.1444	0.7359	0.7779	0.1020
PIM	0.6125	0.6627	0.1506	0.7502	0.7895	0.0969
DyToast	0.6317	0.6822	0.1421	0.7456	0.7858	0.0981
JCLRNT	0.6352	0.6871	0.1405	0.7526	0.7908	0.0958
START	0.6421	<u>0.6903</u>	<u>0.1397</u>	<u>0.7559</u>	<u>0.7954</u>	<u>0.0931</u>
JGRM	0.6357	0.6854	0.1416	0.7533	0.7934	0.0962
TRACK	<u>0.6455</u>	0.6898	0.1402	0.7549	0.7951	0.0927
GREEN	0.6302	0.6811	0.1438	0.7428	0.7824	0.1014
CORE	0.6814	0.7290	0.1283	0.7619	0.8017	0.0934
Improvement(%)	5.56	5.61	8.16	0.79	0.79	-0.76

Methods	Xi'an			Porto		
	τ ↑	ρ ↑	MAE↓	τ ↑	ρ ↑	MAE↓
HRNR	0.6972	0.7459	0.1062	0.7932	0.8226	0.1206
Toast	0.6894	0.7419	0.1094	0.7858	0.8173	0.1186
PIM	0.7022	<u>0.7521</u>	<u>0.1038</u>	0.7901	0.8206	0.1213
DyToast	0.6975	0.7483	0.1058	0.7931	0.8232	0.1245
JCLRNT	0.7024	0.7518	0.1039	0.7949	0.8248	0.1190
START	0.6985	0.7481	0.1047	<u>0.8036</u>	<u>0.8325</u>	<u>0.1172</u>
JGRM	0.6982	0.7467	0.1051	0.7984	0.8280	0.1183
TRACK	0.6998	0.7480	0.1044	0.8025	0.8319	0.1179
GREEN	0.6969	0.7478	0.1041	0.7956	0.8255	0.1186
CORE	0.7129	0.7630	0.1007	0.8267	0.8511	0.1103
Improvement(%)	1.49	1.45	2.99	2.87	2.23	5.89

\mathcal{Q}' . The objective of this task is to accurately retrieve the detoured counterpart from $\mathcal{Q}' \cup \mathcal{D}$ for each query trajectory in \mathcal{Q} . We set $|\mathcal{Q}| = 5000$ and $|\mathcal{D}| = 50000$, and compute similarity in the learned embedding space via cosine similarity. We evaluate with HR@ k (HR@1, HR@5) and mean reciprocal rank (MRR). As shown in Table V, CORE achieves the best performance, as its capture of route choice semantics sharpens trajectory discrimination.

4) *Destination Prediction*: This task aims to predict a trajectory's destination from partial observations [39]. Specifically, given the first 50% of a trajectory, the model predicts the terminal road segment with learning guided by a cross-entropy loss. To avoid information leakage, destination-

TABLE VIII
EVALUATION ON TRAJECTORY GENERATION TASK.

Methods	Beijing			Chengdu		
	Hausdorff↓	DTW↓	EDR↓	Hausdorff↓	DTW↓	EDR↓
TS-TrajGen	0.9535	18.9531	0.6395	0.2067	2.5042	0.3651
STEGA	0.6931	11.5059	0.5001	0.1597	1.5372	0.2987
HOSER	<u>0.5623</u>	<u>7.3345</u>	<u>0.4568</u>	<u>0.1300</u>	<u>1.0188</u>	<u>0.2495</u>
CORE	0.4395	5.8033	0.3511	0.1102	0.8371	0.2082
Improvement(%)	21.84	20.88	23.14	15.23	17.83	16.55

Methods	Xi'an			Porto		
	Hausdorff↓	DTW↓	EDR↓	Hausdorff↓	DTW↓	EDR↓
TS-TrajGen	0.3258	4.8951	0.3689	0.7158	19.2583	0.6899
STEGA	0.2557	3.4756	0.3104	1.0532	16.0175	0.6659
HOSER	<u>0.2481</u>	<u>3.4005</u>	<u>0.2978</u>	<u>0.5697</u>	<u>13.4901</u>	<u>0.5395</u>
CORE	0.2093	2.8187	0.2477	0.4592	10.5123	0.4259
Improvement(%)	15.64	17.11	16.82	19.40	22.07	21.06

dependent terms (i.e., *journey progression* and navigational factors) are computed with respect to the endpoint of the observed 50% prefix. As shown in Table VI, CORE achieves the best performance. Moreover, CORE yields significant gains in Beijing compared to the best-performing baseline, while improvements in the other three cities are modest. We attribute this to road network complexity: Beijing’s more intricate road network topology makes destination prediction harder, whereas simpler networks elsewhere allow baselines to approach performance ceilings.

5) *Path Ranking*: This task assigns each candidate trajectory between a fixed OD pair a score in the range $[0, 1]$, where higher scores indicate greater similarity to the “optimal” path [67]. We generate the top- k candidate paths (here, $k = 10$) and use each path’s IoU with the ground-truth path as the regression target. The model is optimized with MSE loss, and evaluated using Kendall’s τ [68], Spearman’s ρ [69], and MAE. Results in Table VII show that CORE ranks paths more accurately than the baselines, mainly because it better captures route choice semantics and thus more clearly distinguishes the optimal route from less probable alternatives.

6) *Trajectory Generation*: This task aims to generate trajectories that resemble real-world ones. We adopt a search-based paradigm [64] and train the model with a next road segment prediction objective. We quantify similarity to real trajectories using Hausdorff [70], DTW [71], and EDR [72]. As shown in Table VIII, explicitly capturing route choice semantics yields huge improvements over the baselines, underscoring CORE’s potential for real-world trajectory generation.

C. Ablation Studies (RQ2)

To quantify the contribution of each module, we conduct a series of ablation experiments. The corresponding results are summarized in Figure 5. For brevity, we report a single representative metric for each task.

1) *Impact of Environment Perception Module*: (a) *w/ raw POI text*: this variant directly concatenates the POI’s category, subcategory, and name to derive environmental semantics via text embedding. (b) *w/o LLM reasoning*: it bypasses the LLM inference process and directly inputs the prompt into the text embedding model. (c) *w/o fine-grained*: this variant removes fine-grained semantic modeling. (d) *w/o coarse-grained*: it

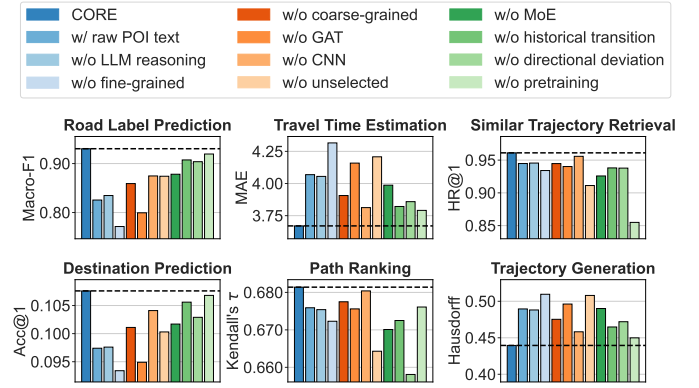


Fig. 5. Performance comparison of CORE and its ablated variants on the Beijing dataset (refer to Appendix B-A for other datasets).

removes coarse-grained environmental semantic modeling. (e) *w/o GAT*: this setting ablates the GAT in fine-grained semantic modeling, so the environmental semantics of *critical segments* no longer propagate. (f) *w/o CNN*: it removes the convolutional layers in coarse-grained environmental semantic modeling, thereby ignoring the contextual influence of *functional hotspots*. Among these variants, *w/ raw POI text* and *w/o LLM reasoning* incur substantial performance degradation, highlighting the LLM’s pivotal role in extracting environmental semantics. Eliminating the fine-grained branch or its GAT also leads to substantial performance drops, whereas removing the coarse-grained branch or its CNN has a comparatively smaller impact. This suggests fine-grained semantics are crucial for expressive representations, while the coarse-grained branch provides useful but secondary cues.

2) *Impact of Route Choice Encoder*: (a) *w/o unselected*: it does not model unselected adjacent road segments. (b) *w/o MoE*: this variant replaces MoE with MLPs using the same activation parameters. (c) *w/o historical transition*: this variant removes the *historical transition likelihood* $P(r_c | r_i)$. (d) *w/o directional deviation*: it removes the *destination-oriented directional deviation* $\Delta\theta_{r_c}$. The results show that the variants *w/o unselected* and *w/o MoE* exhibit the most substantial performance degradation, indicating that jointly modeling semantics from both selected and unselected segments and employing the MoE architecture is crucial for capturing route choice patterns. Removing *historical transition* or *directional deviation* also consistently harms performance, highlighting the complementary importance of these navigational factors.

3) *Impact of Pretraining*: (a) *w/o pretraining*: this variant removes the contrastive pretraining stage. The resulting performance drop across all tasks, particularly in *similar trajectory retrieval*, confirms that the contrastive objective is critical for shaping a discriminative embedding space.

D. Efficiency Analysis (RQ3)

In this subsection, we evaluate the efficiency of CORE from three complementary perspectives: (1) *Data Efficiency*, which assesses the model’s performance under data-scarce conditions; (2) *Training and Inference Efficiency*, which quantifies the training and inference overhead compared with competitive

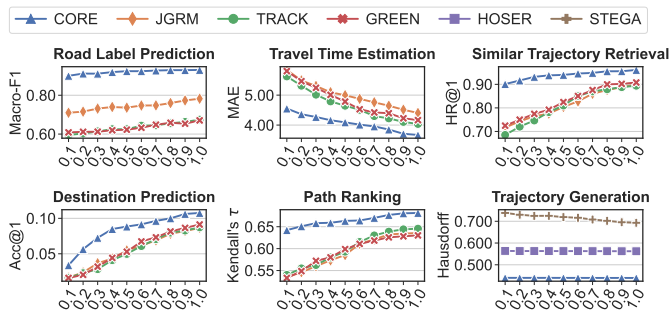


Fig. 6. Results of using varying proportions of training data on the Beijing dataset (refer to Appendix B-B for other datasets).

TABLE IX
AVERAGE TRAINING TIME PER EPOCH (IN HOURS) AND INFERENCE TIME PER TRAJECTORY (IN MILLISECONDS).

Methods	Beijing		Chengdu	
	Training↓	Inference↓	Training↓	Inference↓
JGRM	6.3145	0.7503	0.7432	0.2902
TRACK	1.6134	1.1778	0.2258	0.4055
GREEN	0.5150	0.3191	0.1494	0.1897
CORE	0.8077	0.2785	0.1835	0.1695

Methods	Xi'an		Porto	
	Training↓	Inference↓	Training↓	Inference↓
JGRM	0.7565	0.3144	2.1025	0.5997
TRACK	0.2192	0.4298	0.6207	0.7693
GREEN	0.1428	0.1987	0.4028	0.3538
CORE	0.1708	0.1650	0.4924	0.3049

baselines; and (3) the *Overhead of the LLM-Based Environment Perception Module*, which quantifies the preprocessing cost required for constructing the context-aware road network.

1) *Data Efficiency*: We investigate CORE’s data efficiency by varying the proportion of training data used for pretraining and fine-tuning, and comparing CORE with competitive baselines. The results are shown in Figure 6. We observe that CORE consistently outperforms baselines in the few-shot learning scenarios, demonstrating superior data efficiency. This strong few-shot learning capability primarily stems from CORE’s explicit capturing of context-aware route choice semantics, which injects a powerful inductive bias into the learning process, enabling the model to effectively learn complex trajectory patterns without relying on massive amounts of data.

2) *Training and Inference Efficiency*: Table IX compares the training and inference time of CORE against several competitive baselines. Overall, CORE achieves a favorable trade-off between predictive performance and computational cost. Its training time is slightly longer than GREEN’s but remains moderate and competitive, while at inference, CORE is the most efficient among all compared methods. In contrast, JGRM incurs higher training costs due to the explicit alignment between GPS points and road segments, and TRACK suffers from larger inference latency because it relies on historical traffic states for each trajectory.

3) *Overhead of LLM-Based Environment Perception*: We quantify the preprocessing overhead of the LLM-based Environment Perception Module. Table X reports the API cost and

TABLE X
COMPUTATIONAL OVERHEAD OF THE LLM-BASED ENVIRONMENT PERCEPTION.

Dataset	Input Tokens	Output Tokens	Cost	Time
Beijing	9,581,977	12,912,556	\$2.12	2 h 9 min
Chengdu	2,106,161	2,309,139	\$0.39	23 min
Xi'an	1,683,295	2,158,924	\$0.36	28 min
Porto	948,514	3,098,161	\$0.46	44 min

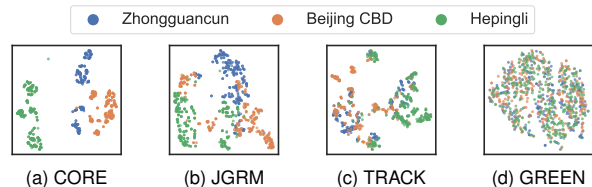


Fig. 7. t-SNE visualization of road segment representations in three representative Beijing areas (Zhongguancun, Beijing CBD, and Hepingli).

time for generating semantic descriptions using Qwen3-8B via OpenRouter⁵ with a concurrency of 32. Notably, even for a megacity such as Beijing with a complex road network, the process incurs a total cost of approximately \$2 and takes about 2 hours. We argue that this one-time cost of constructing a high-quality, semantically rich digital map is computationally and economically feasible.

E. Visualization Analysis (RQ4)

In this subsection, we visually validate CORE from three perspectives: (1) *Road Segment Representations*, which verifies the capture of environmental semantics; (2) *MoE Expert Specialization*, which interprets the learned routing patterns; and (3) *Trajectory Embeddings*, which demonstrates the discriminability of the final representations.

1) *Visualization of Road Segment Representations*: To assess whether CORE effectively captures urban environmental semantics, we visualize the learned road segment embeddings in three representative areas of Beijing: Zhongguancun (commercial district), Beijing CBD (commercial district), and Hepingli (residential district). We apply t-SNE [73] to the road segment embeddings of each method. As shown in Figure 7, the embeddings learned by CORE place Zhongguancun and Beijing CBD close to each other in the t-SNE space while maintaining a clear boundary between them, and both are well separated from Hepingli. This indicates that CORE effectively captures both the semantic similarities and the functional differences across urban environments. In contrast, baselines that rely solely on road network topology or trajectory information, without explicitly modeling urban environmental semantics, fail to distinguish these functional areas, leading to substantial overlap in their representations.

2) *Visualization of MoE Expert Specialization*: To investigate the interpretability of the Route Choice Encoder, we visualize the MoE gating weight distributions in Figure 8. The results reveal distinct context-aware expert specialization across multiple granularities. At the regional level (Figure 8a),

⁵<https://openrouter.ai>

Zhongguancun	0.1015	0.1834	0.1716	0.1022	0.1005	0.1019	0.1365	0.1025
Beijing CBD	0.1013	0.1806	0.1761	0.1033	0.1002	0.1009	0.1016	0.1359
Hepingli	0.1767	0.0911	0.0984	0.0990	0.0736	0.1834	0.1727	0.1051
	0	1	2	3	4	5	6	7

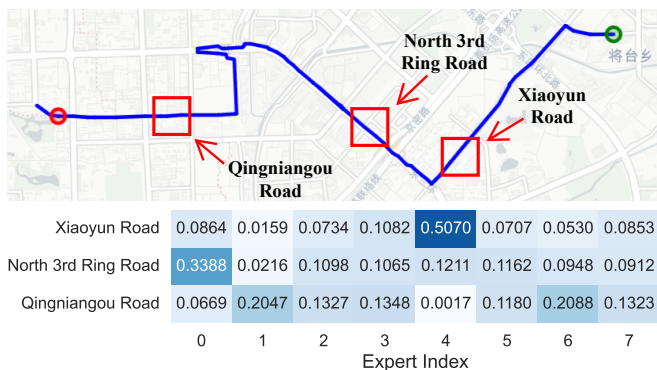
Expert Index

(a) Average expert gating weight across different regions in Beijing.

trunk	0.1643	0.1017	0.1075	0.1016	0.0753	0.1563	0.1424	0.1508
tertiary	0.1001	0.1050	0.1770	0.1749	0.1028	0.1113	0.1192	0.1097
	0	1	2	3	4	5	6	7

Expert Index

(b) Average expert gating weight across different road types in Beijing.

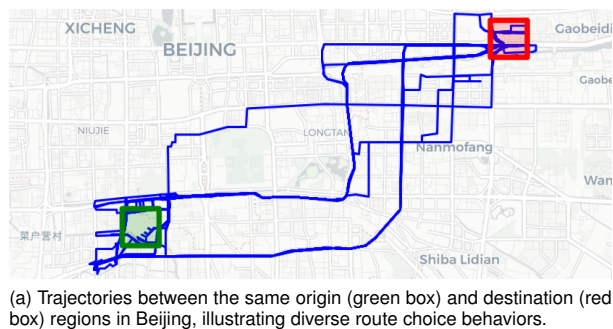


(c) Gating weights of different road segments along a trajectory in Beijing.

Fig. 8. Visualization of MoE gating distributions.

functionally analogous commercial districts (Zhongguancun and Beijing CBD) exhibit consistent expert preferences, which diverge markedly from those of Hepingli, a typical residential district. At the road-type level (Figure 8b), major arterials (road segments whose *highway* tag in OpenStreetMap is *trunk*) and local streets (road segments whose *highway* tag is *tertiary*) are associated with substantially different expert routing patterns. In Figure 8c, we further examine a representative trajectory and report gating weights on three road segments with distinct environments: Xiaoyun Road, an urban arterial adjacent to high-density residential areas; the North 3rd Ring Road, a major urban traffic corridor with very high volume; and Qingniangou Road, a local street in the historic city center. The MoE activates markedly different experts across these segments. Together, these observations indicate that the MoE captures meaningful, context-aware expert specialization that is well aligned with urban semantics.

3) *Visualization of Learned Trajectory Embeddings*: Finally, we investigate whether CORE yields behaviorally informative trajectory embeddings. We select real trajectories exhibiting diverse route patterns between the same origin and destination areas in Beijing, and visualize the trajectory embeddings produced by each method using t-SNE [73], as shown in Figure 9. The embeddings generated by the baseline models exhibit substantial overlap and strong entanglement in the t-SNE space, which obscures differences in route choices. In contrast, the embeddings learned by CORE show markedly clearer separation among distinct route choice behaviors.



(a) Trajectories between the same origin (green box) and destination (red box) regions in Beijing, illustrating diverse route choice behaviors.

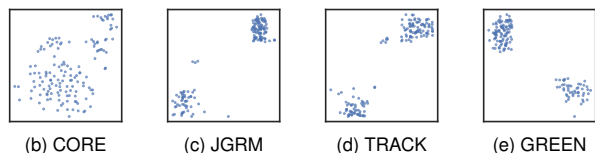


Fig. 9. t-SNE visualization of trajectory embeddings for trajectories sharing the same origin and destination areas in Beijing.

Road Label Prediction (Macro-F1)			Travel Time Estimation (MAE)			Similar Trajectory Retrieval (HR@1)				
δ	50m	0.9079	0.9209	0.9278	3.6614	3.6651	3.6714	0.9502	0.9564	0.9610
	100m	0.9143	0.9303	0.9088	3.6672	3.6703	3.6704	0.9581	0.9611	0.9601
	200m	0.9228	0.9141	0.9032	3.6581	3.6687	3.6690	0.9589	0.9598	0.9587
		500m	1000m	2000m	500m	1000m	2000m	500m	1000m	2000m
Destination Prediction (Acc@1)			Path Ranking (Kendall's τ)			Trajectory Generation (Hausdorff)				
δ	50m	0.1074	0.1065	0.1071	0.6812	0.6815	0.6808	0.4397	0.4395	0.4392
	100m	0.1082	0.1076	0.1075	0.6812	0.6814	0.6810	0.4396	0.4395	0.4394
	200m	0.1079	0.1073	0.1070	0.6814	0.6811	0.6807	0.4392	0.4395	0.4393
		500m	1000m	2000m	500m	1000m	2000m	500m	1000m	2000m

Fig. 10. Sensitivity of CORE to spatial perception scale hyperparameters (δ and L) on the Beijing dataset (refer to Appendix B-C1 for other datasets).

These results suggest that, by explicitly capturing context-aware route choice semantics, CORE substantially enhances the discriminability of fine-grained route choice differences and produces trajectory representations that are more informative for downstream tasks.

F. Sensitivity Analyses (RQ5)

In this subsection, we systematically examine the robustness of CORE from three perspectives: (1) *Hyperparameter Sensitivity*, which studies how spatial perception scales and the critical-segment selection ratio affect model performance; (2) *Sensitivity to LLM Backbone*, which investigates how different LLMs used in the Environment Perception Module influence downstream results; and (3) *Sensitivity to POI Completeness*, which evaluates how CORE behaves under varying degrees of POI sparsity in practical settings.

1) *Hyperparameter Sensitivity*: In our Environment Perception Module, two hyperparameters jointly determine the spatial scale of semantic perception: (1) the POI perception radius δ

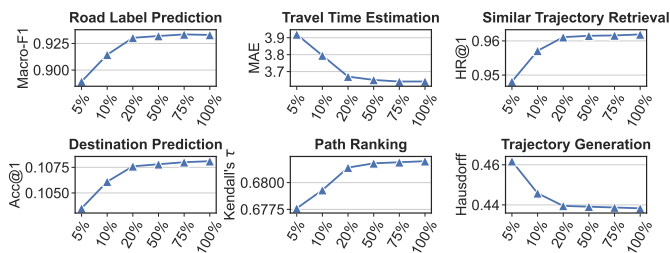


Fig. 11. Impact of the critical segment selection ratio η on the Beijing dataset (refer to Appendix B-C1 for other datasets).

TABLE XI
PERFORMANCE OF CORE WITH DIFFERENT LLM BACKBONES.

LLM Backbone	Macro-F1 \uparrow	MAE \downarrow	HR@1 \uparrow	Acc@1 \uparrow	Kendall's τ \uparrow	Hausdorff \downarrow	
Beijing	CORE w/ Qwen3-0.6B	0.8872	3.7881	0.9498	0.1039	0.6781	0.4563
	CORE w/ Qwen3-8B	<u>0.9303</u>	3.6703	<u>0.9611</u>	0.1076	0.6814	<u>0.4395</u>
	CORE w/ DeepSeek-V3.2-Exp	0.9312	<u>3.6706</u>	0.9614	<u>0.1075</u>	<u>0.6813</u>	0.4393
Chengdu	CORE w/ Qwen3-0.6B	0.8182	1.3837	0.9218	0.4267	0.7601	0.1201
	CORE w/ Qwen3-8B	0.8574	<u>1.3681</u>	<u>0.9402</u>	0.4296	<u>0.7619</u>	<u>0.1102</u>
	CORE w/ DeepSeek-V3.2-Exp	<u>0.8541</u>	1.3675	0.9408	<u>0.4294</u>	0.7622	0.1098
Xi'an	CORE w/ Qwen3-0.6B	0.8163	2.1934	0.9399	0.3589	0.7067	0.2285
	CORE w/ Qwen3-8B	<u>0.8456</u>	<u>2.1498</u>	0.9540	0.3631	<u>0.7129</u>	0.2093
	CORE w/ DeepSeek-V3.2-Exp	0.8472	<u>2.1475</u>	<u>0.9536</u>	<u>0.3627</u>	0.7131	<u>0.2097</u>
Porto	CORE w/ Qwen3-0.6B	0.7693	1.4029	0.9587	0.1706	0.8056	0.4793
	CORE w/ Qwen3-8B	<u>0.8073</u>	<u>1.3519</u>	0.9746	<u>0.1734</u>	0.8267	<u>0.4592</u>
	CORE w/ DeepSeek-V3.2-Exp	0.8089	1.3493	<u>0.9738</u>	0.1739	<u>0.8265</u>	0.4587

(default 100 m) for fine-grained semantic modeling, and (2) the grid side length L (default 1000 m) for coarse-grained semantic modeling. Although these hyperparameters modulate the perception granularity, a robust model should retain stable performance over a reasonable range of their values rather than rely on a specific configuration. To assess this robustness, we vary δ within $\{50 \text{ m}, 100 \text{ m}, 200 \text{ m}\}$ and L within $\{500 \text{ m}, 1000 \text{ m}, 2000 \text{ m}\}$. As shown in Figure 10, CORE consistently exhibits strong performance across all configurations, indicating that it is not sensitive to these hyperparameter choices and confirming the model's stability.

We further evaluate the effectiveness of restricting fine-grained LLM-based semantic modeling to high-traffic *critical segments*. We conduct a sensitivity analysis on the selection ratio $\eta \in \{5\%, 10\%, 20\%, 50\%, 75\%, 100\%\}$. As shown in Figure 11, increasing η from 5% to 20% yields substantial gains across all downstream tasks, indicating that fine-grained environmental semantic modeling on frequently visited segments is crucial for capturing key behavioral patterns. However, further increasing η beyond 20% leads to saturated improvements. This observation is consistent with the long-tailed distribution of urban road-network visitation, where a small subset of core segments accounts for most traffic interactions and semantic information, suggesting that designating the top 20% of segments as *critical segments* offers a favorable trade-off between performance and computational cost.

2) *Sensitivity to LLM backbone*: We further examine the sensitivity of CORE to the choice of LLM backbone, with results reported in Table XI, where we use one representative metric per task. When we scale down the backbone from Qwen3-8B to Qwen3-0.6B, the performance consistently decreases across all metrics, indicating that an overly small

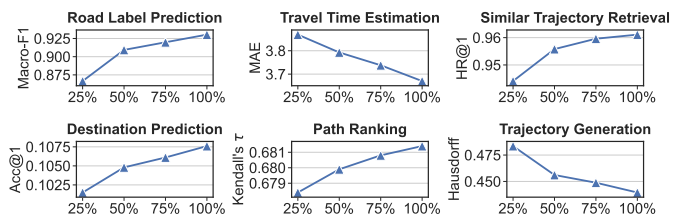


Fig. 12. Sensitivity of CORE to POI completeness on the Beijing dataset (refer to Appendix B-C2 for other datasets).

LLM is insufficient to capture the required semantic reasoning over POI distributions. In contrast, replacing Qwen3-8B with DeepSeek-V3.2-Exp, a substantially larger model with 671B parameters, brings almost no performance improvement across all metrics, suggesting that a medium-sized LLM is sufficient and strikes a favorable balance between accuracy and computational cost in our setting.

3) *Sensitivity to POI Completeness*: In practical applications, limited POI sources and collection constraints often lead to incomplete or sparse POI data. To assess the robustness of CORE under such conditions, we randomly subsample the original POI database with $\gamma \in \{25\%, 50\%, 75\%, 100\%\}$ and retrain the model. As shown in Figure 12, CORE's performance decreases as POI completeness declines, confirming its dependence on environmental data richness. Nevertheless, CORE does not undergo catastrophic failure even under severe sparsity (e.g., with only 25% of POIs). This indicates that although missing POI data hinders the precise extraction of environmental semantics, the LLM-based module leverages its broad world knowledge to infer reasonable semantic approximations from sparse clues, thereby partially mitigating the impact of data sparsity on performance.

VI. CONCLUSION

In this paper, we propose CORE, a TRL framework that injects context-aware route choice semantics into trajectory representations. CORE leverages an LLM-based Environment Perception Module to construct a context-enriched road network and employs an MoE-based Route Choice Encoder to capture complex routing patterns. Extensive experiments on four real-world datasets demonstrate that CORE consistently outperforms *state-of-the-art* baselines while exhibiting superior data and computational efficiency.

Despite these strengths, CORE is currently limited to single-city modeling and therefore cannot directly transfer the learned semantics to other urban areas without retraining. In future work, we plan to develop a trajectory foundation model. By distilling universal knowledge about the interactions between environment and behavior from large-scale data, we aim to achieve robust generalization and enable zero-shot transfer to previously unseen urban environments.

REFERENCES

- [1] Y. Zheng, "Trajectory data mining: an overview," *ACM Trans. Intell. Syst. Technol.*, 2015.
- [2] S. Wang, Z. Bao, J. S. Culpepper, and G. Cong, "A survey on trajectory data management, analytics, and learning," *ACM Comput. Surv.*, 2021.

- [3] S. Wang, J. Cao, and P. S. Yu, "Deep learning for spatio-temporal data mining: A survey," *IEEE Trans. Knowl. Data Eng.*, 2022.
- [4] J. J. Yu, "Citywide estimation of travel time distributions with bayesian deep graph learning," *IEEE Trans. Knowl. Data Eng.*, 2023.
- [5] C. Zhang, K. Zhao, and M. Chen, "Beyond the limits of predictability in human mobility prediction: Context-transition predictability," *IEEE Trans. Knowl. Data Eng.*, 2023.
- [6] D. Hu, L. Chen, H. Fang, Z. Fang, T. Li, and Y. Gao, "Spatio-temporal trajectory similarity measures: A comprehensive survey and quantitative study," *IEEE Trans. Knowl. Data Eng.*, 2024.
- [7] Z. Mao, Z. Li, D. Li, L. Bai, and R. Zhao, "Jointly contrastive representation learning on road network and trajectory," in *CIKM*, 2022.
- [8] S. B. Yang, J. Hu, C. Guo, B. Yang, and C. S. Jensen, "Lightpath: Lightweight and scalable path representation learning," in *SIGKDD*, 2023.
- [9] J. Jiang, D. Pan, H. Ren, X. Jiang, C. Li, and J. Wang, "Self-supervised trajectory representation learning with temporal regularities and travel semantics," in *ICDE*, 2023.
- [10] T.-Y. Fu and W.-C. Lee, "Trembr: Exploring road networks for trajectory representation learning," *ACM Trans. Intell. Syst. Technol.*, 2020.
- [11] S. B. Yang, C. Guo, J. Hu, J. Tang, and B. Yang, "Unsupervised path representation learning with curriculum negative sampling," in *IJCAI*, 2021.
- [12] S. Hochreiter and J. Schmidhuber, "Long short-term memory," *Neural Comput.*, 1997.
- [13] K. Cho *et al.*, "Learning phrase representations using rnn encoder-decoder for statistical machine translation," in *EMNLP*, 2014.
- [14] A. Vaswani *et al.*, "Attention is all you need," in *NeurIPS*, 2017.
- [15] Y. Chen *et al.*, "Robust road network representation learning: When traffic patterns meet traveling semantics," in *CIKM*, 2021.
- [16] P. Veličković, G. Cucurull, A. Casanova, A. Romero, P. Lio, and Y. Bengio, "Graph attention networks," in *ICLR*, 2018.
- [17] S. Zhou, S. Shang, L. Chen, P. Han, and C. S. Jensen, "Grid and road expressions are complementary for trajectory representation learning," in *SIGKDD*, 2025.
- [18] C. G. Prato, "Route choice modeling: past, present and future research directions," *Journal of Choice Modelling*, 2009.
- [19] A. Lima, R. Stanojevic, D. Papagiannaki, P. Rodriguez, and M. C. González, "Understanding individual routing behaviour," *Journal of The Royal Society Interface*, 2016.
- [20] D. Dai *et al.*, "Deepseekmo: Towards ultimate expert specialization in mixture-of-experts language models," in *ACL*, 2024.
- [21] T. Chen, S. Kornblith, M. Norouzi, and G. Hinton, "A simple framework for contrastive learning of visual representations," in *ICML*, 2020.
- [22] X. Li, K. Zhao, G. Cong, C. S. Jensen, and W. Wei, "Deep representation learning for trajectory similarity computation," in *ICDE*, 2018.
- [23] D. Yao, G. Cong, C. Zhang, and J. Bi, "Computing trajectory similarity in linear time: A generic seed-guided neural metric learning approach," in *ICDE*, 2019.
- [24] P. Han, J. Wang, D. Yao, S. Shang, and X. Zhang, "A graph-based approach for trajectory similarity computation in spatial networks," in *SIGKDD*, 2021.
- [25] D. Wang, J. Zhang, W. Cao, J. Li, and Y. Zheng, "When will you arrive? estimating travel time based on deep neural networks," in *AAAI*, 2018.
- [26] Z. Wang, K. Fu, and J. Ye, "Learning to estimate the travel time," in *SIGKDD*, 2018.
- [27] X. Fang, J. Huang, F. Wang, L. Zeng, H. Liang, and H. Wang, "Constgat: Contextual spatial-temporal graph attention network for travel time estimation at baidu maps," in *SIGKDD*, 2020.
- [28] S. Zhou, S. Shang, L. Chen, C. S. Jensen, Jensen, and P. Kalnis, "Red: Effective trajectory representation learning with comprehensive information," in *VLDB*, 2025.
- [29] Z. Ma *et al.*, "More than routing: Joint gps and route modeling for refine trajectory representation learning," in *WWW*, 2024.
- [30] J. Devlin, M.-W. Chang, K. Lee, and K. Toutanova, "Bert: Pre-training of deep bidirectional transformers for language understanding," in *NAACL*, 2019.
- [31] C. Han *et al.*, "Bridging traffic state and trajectory for dynamic road network and trajectory representation learning," in *AAAI*, 2025.
- [32] M.-x. Wang, W.-C. Lee, T.-y. Fu, and G. Yu, "Learning embeddings of intersections on road networks," in *SIGSPATIAL*, 2019.
- [33] M.-X. Wang, W.-C. Lee, T.-Y. Fu, and G. Yu, "On representation learning for road networks," *ACM Trans. Intell. Syst. Technol.*, 2020.
- [34] A. Grover and J. Leskovec, "node2vec: Scalable feature learning for networks," in *SIGKDD*, 2016.
- [35] Y. Chen, X. Li, G. Cong, Z. Bao, and C. Long, "Semantic-enhanced representation learning for road networks with temporal dynamics," *arXiv preprint arXiv:2403.11495*, 2024.
- [36] Z. Wu, S. Pan, F. Chen, G. Long, C. Zhang, and P. S. Yu, "A comprehensive survey on graph neural networks," *IEEE Trans. Neural Netw. Learn. Syst.*, 2020.
- [37] T. S. Jepsen, C. S. Jensen, and T. D. Nielsen, "Relational fusion networks: Graph convolutional networks for road networks," *IEEE Trans. Intell. Transp. Syst.*, 2020.
- [38] T. N. Kipf and M. Welling, "Semi-supervised classification with graph convolutional networks," in *ICLR*, 2017.
- [39] N. Wu, X. W. Zhao, J. Wang, and D. Pan, "Learning effective road network representation with hierarchical graph neural networks," in *SIGKDD*, 2020.
- [40] L. Zhang and C. Long, "Road network representation learning: A dual graph-based approach," *ACM Trans. Knowl. Discov. Data*, 2023.
- [41] A. Antelmi, G. Cordasco, M. Polato, V. Scarano, C. Spagnuolo, and D. Yang, "A survey on hypergraph representation learning," *ACM Comput. Surv.*, 2023.
- [42] Y. Chang, E. Tanin, X. Cao, and J. Qi, "Spatial structure-aware road network embedding via graph contrastive learning," in *EDBT*, 2023.
- [43] Y. Zhu, Y. Xu, F. Yu, Q. Liu, S. Wu, and L. Wang, "Graph contrastive learning with adaptive augmentation," in *WWW*, 2021.
- [44] L. Ouyang *et al.*, "Training language models to follow instructions with human feedback," in *NeurIPS*, 2022.
- [45] J. Wang *et al.*, "Large language models as urban residents: An llm agent framework for personal mobility generation," in *NeurIPS*, 2024.
- [46] C. Shao *et al.*, "Chain-of-planned-behaviour workflow elicits few-shot mobility generation in llms," *arXiv preprint arXiv:2402.09836*, 2024.
- [47] J. Feng, Y. Du, J. Zhao, and Y. Li, "Agentmove: Predicting human mobility anywhere using large language model based agentic framework," *arXiv preprint arXiv:2408.13986*, 2024.
- [48] L. Gong *et al.*, "Mobility-llm: Learning visiting intentions and travel preference from human mobility data with large language models," in *NeurIPS*, 2024.
- [49] P. Li, M. de Rijke, H. Xue, S. Ao, Y. Song, and F. D. Salim, "Large language models for next point-of-interest recommendation," in *SIGIR*, 2024.
- [50] J. Cheng *et al.*, "Poi-enhancer: An llm-based semantic enhancement framework for poi representation learning," in *AAAI*, 2025.
- [51] Z. Zhang *et al.*, "Promptst: Prompt-enhanced spatio-temporal multi-attribute prediction," in *CIKM*, 2023.
- [52] Z. Li *et al.*, "Urbangpt: Spatio-temporal large language models," in *SIGKDD*, 2024.
- [53] Y. Yuan, J. Ding, J. Feng, D. Jin, and Y. Li, "Unist: A prompt-empowered universal model for urban spatio-temporal prediction," in *SIGKDD*, 2024.
- [54] Z. Zhou *et al.*, "Trajcn: Leveraging llms for cognizing movement patterns and travel purposes from trajectories," in *IJCAI*, 2025.
- [55] B. Hillier and J. Hanson, *The social logic of space*. Cambridge University Press, 1989.
- [56] A. Yang *et al.*, "Qwen3 technical report," *arXiv preprint arXiv:2505.09388*, 2025.
- [57] Y. Zhang *et al.*, "Qwen3 embedding: Advancing text embedding and reranking through foundation models," *arXiv preprint arXiv:2506.05176*, 2025.
- [58] C. D. Harris and E. L. Ullman, "The nature of cities," *The annals of the American academy of political and social science*, 1945.
- [59] J. Yuan, Y. Zheng, and X. Xie, "Discovering regions of different functions in a city using human mobility and pois," in *SIGKDD*, 2012.
- [60] G. Boeing, "Modeling and analyzing urban networks and amenities with osmnx," *Geographical Analysis*, 2025.
- [61] C. Yang and G. Gidofalvi, "Fast map matching, an algorithm integrating hidden markov model with precomputation," *Int. J. Geogr. Inf. Sci.*, 2018.
- [62] W. Jiang, W. X. Zhao, J. Wang, and J. Jiang, "Continuous trajectory generation based on two-stage gan," in *AAAI*, 2023.
- [63] Y. Wang, J. Cao, W. Huang, Z. Liu, T. Zheng, and M. Song, "Spatiotemporal gated traffic trajectory simulation with semantic-aware graph learning," *Inf. Fusion*, 2024.
- [64] J. Cao *et al.*, "Holistic semantic representation for navigational trajectory generation," in *AAAI*, 2025.
- [65] I. Loshchilov and F. Hutter, "Decoupled weight decay regularization," in *ICLR*, 2019.
- [66] L. Wang, H. Gao, C. Zhao, X. Sun, and D. Dai, "Auxiliary-loss-free load balancing strategy for mixture-of-experts," *arXiv preprint arXiv:2408.15664*, 2024.

- [67] S. B. Yang, C. Guo, and B. Yang, "Context-aware path ranking in road networks," *IEEE Trans. Knowl. Data Eng.*, 2022.
- [68] M. G. Kendall, "A new measure of rank correlation," *Biometrika*, 1938.
- [69] C. Spearman, "The proof and measurement of association between two things," *Am. J. Psychol.*, 1904.
- [70] D. Xie, F. Li, and J. M. Phillips, "Distributed trajectory similarity search," in *VLDB*, 2017.
- [71] E. Keogh, "Exact indexing of dynamic time warping," in *VLDB*, 2002.
- [72] L. Chen, M. T. Özsu, and V. Oria, "Robust and fast similarity search for moving object trajectories," in *SIGMOD*, 2005.
- [73] L. v. d. Maaten and G. Hinton, "Visualizing data using t-sne," *J. Mach. Learn. Res.*, 2008.

SUPPLEMENTARY MATERIAL

CAPTURING CONTEXT-AWARE ROUTE CHOICE SEMANTICS FOR TRAJECTORY REPRESENTATION LEARNING

APPENDIX A

DETAILS OF ENVIRONMENT PERCEPTION MODULE

A. Prompts for Fine-Grained Semantic Modeling

At the fine-grained level, the objective is to generate detailed descriptions of individual road segments by summarizing the POI context surrounding them. The prompt template fed into the LLM consists of the following components:

- *Role Definition*: The LLM is prompted to assume the role of a resident, encouraging it to produce contextually grounded and locally nuanced descriptions.
- *Structured POI Data Input*: A structured list of nearby POIs is provided as factual grounding for the description.
- *Task Instruction*: The LLM is explicitly instructed to generate a description of the road segment based on the given information.

LLM Prompt Template (Fine-Grained Semantic Modeling).

You are a resident living in `<city_name>`, familiar with the local transportation network and surrounding POI information.

There is a road segment with the following POIs located within a 100-meter radius:

`<poi_count>` POIs categorized under [`<poi_category>`], further subdivided as:

- `<poi_count>` [`<poi_subcategory>`]: `<poi_name_list>`
- `<poi_count>` [`<poi_subcategory>`]: `<poi_name_list>`
- ... (Can be further expanded here)

... (Additional primary categories may be added in the same format)

Please describe the relevant characteristics of this road section based on the POI information within a 100-meter radius around it.

To illustrate the applicability of the proposed template, we present a case study of a road segment on Qianmen East Street, which is located in a historically and commercially significant area of Beijing frequented by both residents and tourists.

Illustrative Prompt Instance (Fine-Grained Semantic Modeling).

You are a resident living in `Beijing`, familiar with the local transportation network and surrounding POI information.

There is a road segment with the following POIs located within a 100-meter radius:

6 POIs categorized under [`Shopping Services`], further subdivided as:

- 2 [`Clothing & Shoes Stores`]: `Fashion Frontline (Xinjiekou Street)`, `Old Beijing Cloth Shoes (Qianmen West Houheyuan Street)`.
- 2 [`Specialty Stores`]: `Gaojiazhai Grocery`, `Beijing Specialty Store (Qianmen West Heyan Community)`.
- 2 [`Convenience Stores`]: `Lehafu Supermarket`, `Cigarettes & Cold Drinks`.

4 POIs categorized under [`Catering Services`], further subdivided as:

- 1 [`Food-Related Establishment`]: `Juewei Taiwanese Salt & Pepper Chicken`.
- 2 [`Chinese Restaurants`]: `Mian Ai Mian (Qianmen Branch)`, `Qipin Xiang Tofu`.
- 1 [`Fast Food Restaurant`]: `KFC (Qianmen Branch)`.

1 POIs categorized under [`Transportation Facilities`], further subdivided as:

- 1 [`Subway Station`]: `Qianmen Subway Station (Southwest Exit C)`.

1 POIs categorized under [`Government & Social Organizations`], further subdivided as:

- 1 [`Public Security Institution`]: `Dashilan Patrol Police Station`.

1 POIs categorized under [`Healthcare Services`], further subdivided as:

- 1 [`Healthcare Facility`]: `Blood Donation Cabin`.

2 POIs categorized under [`Accommodation Services`], further subdivided as:

- 2 [`Hotel`]: `Qianmen Guanqi Hotel (Qianmen East Branch)`, `Shunchalong Hotel`.

Please describe the relevant characteristics of this road section based on the POI information within a 100-meter radius around it.

LLM-Generated Description (Fine-Grained Semantic Modeling).

Based on POI information within 100 meters of this road section, the area has the following characteristics:

1. Vibrant Commerce and Diverse Consumption Scenes

- **Dense Shopping Services:** Six shopping-related POIs form a commercial belt focused on clothing, shoes, specialty retail, and convenience stores.
- **Blend of Fashion and Tradition:** Stores such as “Fashion Frontline (Xinjiekou Street)” and “Old Beijing Cloth Shoes (Qianmen West Houheyan Street)” combine modern trends with local culture, attracting young people and tourists.
- **Convenience Meets Specialty:** Convenience stores like “Lehafu Supermarket” and “Cigarettes & Cold Drinks” meet daily needs, while specialty shops like “Gaojiazhai Grocery” and “Beijing Specialty Store (Qianmen West Heyan Community)” offer local products favored by tourists seeking souvenirs.
- **Varied Dining Options:** Four food-related POIs cover fast food, Chinese cuisine, and specialty snacks, creating an all-day dining scene.
- **Local and International Flavors:** Restaurants like “Mian Ai Mian (Qianmen Branch)” and “Qipin Xiang Tofu” specialize in Beijing cuisine, while “KFC (Qianmen Branch)” and “Juewei Taiwanese Salt & Pepper Chicken” offer quick and convenient meals, catering to both locals and tourists.

2. Transportation Hub and High Foot Traffic

- **Direct Metro Access:** “Qianmen Subway Station (Southwest Exit C)” links subway and ground transport, generating heavy flows during rush hours and serving both commercial and commuting needs.
- **Public Security:** The “Dashilan Police Patrol Station” reflects strict public safety management, enhancing residents’ and visitors’ sense of security.

3. Prominent Tourism and Accommodation Functions

- **Comprehensive Lodging Options:** Hotels such as “Qianmen Guanqi Hotel (Qianmen East Branch)” and “Shunchaolong Hotel” confirm the area as a tourist hotspot, likely near historical and cultural attractions like Qianmen Street.
- **Cultural Experience Extension:** POIs like “Old Beijing Cloth Shoes (Qianmen West Houheyan Street)” and “Beijing Specialty Store” complement the Qianmen historical(cultural district and enhance its tourism appeal.

4. Healthcare and Community Services

- **Blood Donation Cabin:** The blood donation cabin provides basic medical support and public welfare services for residents and tourists, strengthening community functions.

Summary: This road section lies in the **core Qianmen business district**, integrating **commerce, transportation, tourism, and residential** functions, and exemplifying the fusion of Beijing’s historical culture with modern lifestyle. Its dense POIs and diverse services make it a key node for tourists, residents, and commuters, well suited for walking, shopping, leisure, and short-term stays.

As can be seen, given a list of POIs around a road segment (e.g., 6 shopping-related POIs, 4 dining-related POIs), the LLM does more than simply restate this information. Instead, it uses commonsense reasoning to derive abstract functional concepts such as “vibrant commerce and diverse consumption scenes” and “transportation hub and high foot traffic”. This process constitutes a conceptual leap from discrete, low-level features to a high-level, synthesized semantic representation. Notably, these abstract concepts are not present in the raw input features; they are inferred by the LLM using its world knowledge.

B. Prompts for Coarse-Grained Semantic Modeling

At the coarse-grained level, we aim to generate textual descriptions for *functional hotspots* \mathcal{H}_c of POI type c . Similar to the prompt designed for fine-grained POI context described above, this prompt also comprises three components: *Role Definition*, *Structured POI Data Input*, and *Task Instruction*.

LLM Prompt Template (Coarse-Grained Semantic Modeling).

You are a resident living in `<city_name>`, familiar with the local transportation network and surrounding POI information.

In a 1000m × 1000m area of `<city_name>`, POIs of the type `[<poi_category>]` exhibit significant clustering characteristics. Data analysis shows that the number of `[<poi_category>]` POIs in this area ranks within the top 10% in `<city_name>`. Further subdividing these `[<poi_category>]` POIs, they include:

- `<poi_count>` `[<poi_subcategory>]: <poi_name_list>`
- `<poi_count>` `[<poi_subcategory>]: <poi_name_list>`
- ... (Can be further expanded here)

Please describe the characteristics of this 1000m × 1000m area where a large number of `[<poi_category>]` POIs are clustered.

Below we present an example of a functional hotspot of type “Shopping Services” near Beijing CBD.

Illustrative Prompt Instance (Coarse-Grained Semantic Modeling).

You are a resident living in **Beijing**, familiar with the local transportation network and surrounding POI information.

In a 1000m × 1000m area of **Beijing**, POIs of the type [Shopping Services] exhibit significant clustering characteristics. Data analysis shows that the number of [Shopping Services] POIs in this area ranks within the top 10% in **Beijing**. Further subdividing these [Shopping Services] POIs, they include:

- 790 [Specialty Stores]: Li-Ning (Fuli Plaza Store), Dionysus Wine Cellar, Youngor, etc.
 - 80 [Personal Care & Cosmetics Stores]: Qingzhuang Cosmetics, Scent Library, PIFI FACE Perfume, etc.
 - 24 [Sports Goods Stores]: Adidas (China World Trade Center South Zone), Reebok Treadmill Store (Guomao Store), Kingsmith Treadmill Store (Guomao Store), etc.
 - 52 [Convenience Stores]: 7-Eleven (Huamao Store), Quick (Jianwai Branch 2), Wankeyuan Supermarket (Jingheng Street), etc.
 - 40 [Shopping Malls]: Beijing Yintai Center in01, China World Trade Center South Zone, China World Trade Center North Zone, etc.
 - 46 [Home & Building Material Markets]: Dakang Home Furnishing, Risheng Furniture & Hardware, Bairuisi Furniture, etc.
 - 46 [Electronics & Appliance Stores]: Changhong Air Conditioning, ThinkPad Laptop Store, BOSE (China World Trade Center North Zone), etc.
 - 8 [Stationery Stores]: JimmyBlack, 7G Office, Montblanc (China World Trade Center South Zone), etc.
 - 708 [Clothing & Shoes Stores]: Yaliange, Xiu Clothing, Xiaojin Wardrobe (Jianwai SOHO Store), etc.
 - 6 [Auction Houses]: Beijing Jianya Century Auction Co., Ltd., Beijing Zhonghan Auction Co., Ltd., Beijing Zhongzhao International Auction Co., Ltd. (Jintong East Road), etc.
 - 62 [Flower & Pet Markets]: No. 18 Flower Shop, Love Flowers, LOVE Flower Studio, etc.
 - 28 [Supermarkets]: Jingkelong Supermarket, Mannings (Yintai Center Store), CR Vanguard (Guomao Store), etc.
- Please describe the characteristics of this 1000m × 1000m area where a large number of [Shopping Services] POIs are clustered.

LLM-Generated Description (Coarse-Grained Semantic Modeling).

Based on the data, the 1000m × 1000m area shows a highly concentrated commercial profile, summarized as follows:

1. Highly Concentrated, Diverse Business Mix

- **Core Business Types:** Mainly [specialty stores] (790) and [clothing & shoes stores] (708), indicating strong fashion and personalized shopping, likely with brand flagships and boutiques.
- **Supporting Daily Services:** [convenience stores] (52) and [supermarkets] (28) enable one-stop shopping for everyday needs.
- **High-End and Niche Segments:** [electronics & appliance stores] (46), [home & building material markets] (46), and [stationery stores] (8) show that the area also serves professionals and affluent residents.

2. Likely Location: Beijing's Core Commercial Districts

- **POI Name Clues:** Frequent ``Guomao`` in POI names suggests proximity to the Guomao CBD or a similar prime business district.
- **Exceptionally High POI Density:** Nearly 2,000 shopping-related POIs within one square kilometer, far exceeding typical commercial zones, points to a central retail hub such as Guomao, Sanlitun, or Wangjing.

3. Multi-Level Consumption Structure

- **Mass Market Consumption:** Supermarkets and convenience stores address the daily needs of nearby residents.
- **High-End and Niche Consumption:** Stores like ``Dionysus Wine Cellar``, ``Montblanc``, and ``Beijing Jianya Century Auction Co., Ltd.`` reflect luxury brands and specialized services targeting affluent and interest-driven customers.

4. Commercial Vitality Driven by Transit and Foot Traffic

- **Density Backed by Accessibility:** Such POI concentration implies strong transport links (e.g., metro, bus hubs) and high population density (e.g., office towers, housing). ``Guomao`` further hints at a metro hub or major retail cluster.
- **Competitive and Complementary Dynamics:** Coexisting specialty, fashion, and general markets suggest differentiated positioning (e.g., brand vs. value), while services like convenience stores provide complementary functions that enhance overall vitality.

5. Potential Challenges

- **Oversaturation Risk:** High POI density may cause homogeneous competition and pressure on smaller retailers.
- **Traffic Pressure:** Intensive commercial activity can strain surrounding roads, requiring effective traffic planning and management.

Conclusion: The area is most likely a **core commercial district in Beijing** (e.g., Guomao, Sanlitun) or a **large emerging commercial complex**, characterized by:

- **Diverse Business Types:** Covering everyday retail and luxury brands.
- **Broad Consumption Spectrum:** Serving mass, middle-class, and affluent groups.
- **Transit-Oriented Clustering:** High commercial density supported by transit and strong population flows.
- **Potential Functional Zoning:** Distinct commercial ecosystems indicated by specialized POIs.

These results demonstrate that, in coarse-grained semantic modeling, LLMs also utilize their encoded world knowledge to perform powerful spatial pattern recognition. For example, by detecting dense clusters of specialty stores and shopping malls, the model not only identifies the area as a core commercial district of Beijing but also reveals deeper characteristics, such as its multi-level consumption structure and commercial vitality driven by transit and foot traffic.

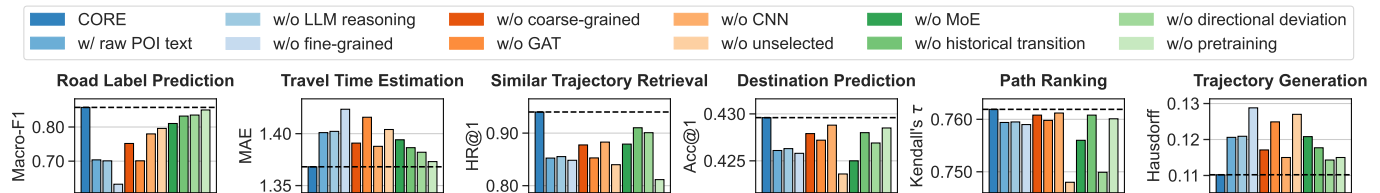


Fig. 13. Performance comparison of CORE and its ablated variants on the Chengdu dataset.

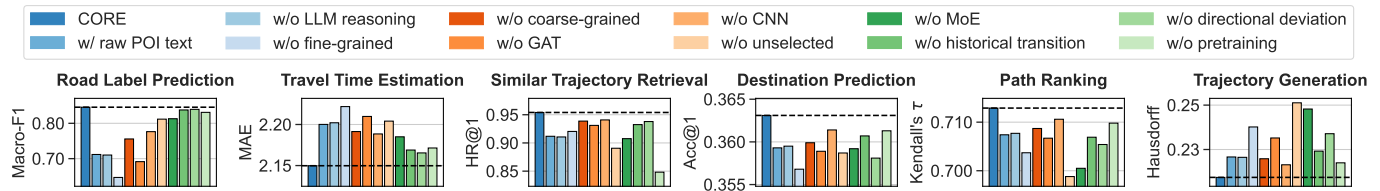


Fig. 14. Performance comparison of CORE and its ablated variants on the Xi'an dataset.

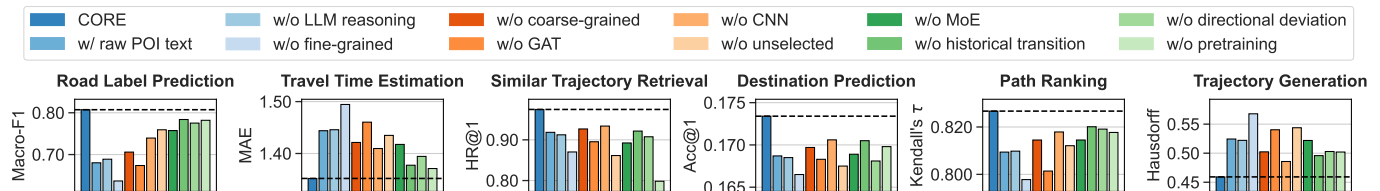


Fig. 15. Performance comparison of CORE and its ablated variants on the Porto dataset.

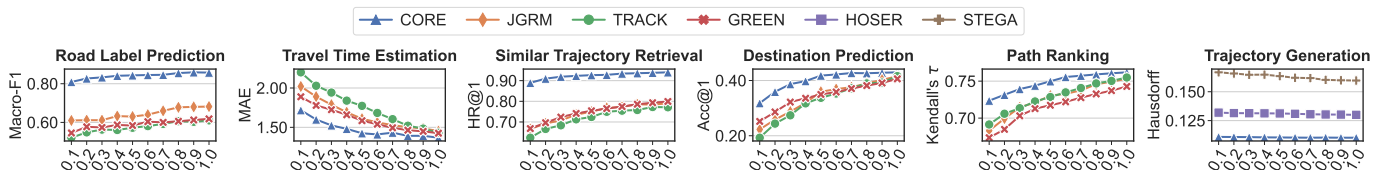


Fig. 16. Results of using varying proportions of training data on the Chengdu dataset.

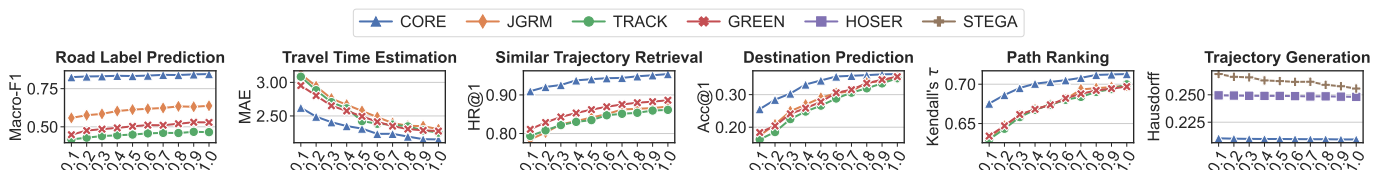


Fig. 17. Results of using varying proportions of training data on the Xi'an dataset.

APPENDIX B ADDITIONAL EXPERIMENTAL RESULTS

A. Ablation Studies

Figures 13 to 15 report additional ablation results on the Chengdu, Xi'an, and Porto datasets. These results exhibit trends that are highly consistent with those observed on the Beijing dataset in the main text, further corroborating the robustness and effectiveness of CORE's core components under different urban contexts.

B. Data Efficiency

Figures 16 to 18 present the data-efficiency results on the Chengdu, Xi'an, and Porto datasets. The observed trends are highly consistent with the results on the Beijing dataset presented in the main text, further demonstrating that CORE reliably maintains strong data efficiency across different cities and data scales.

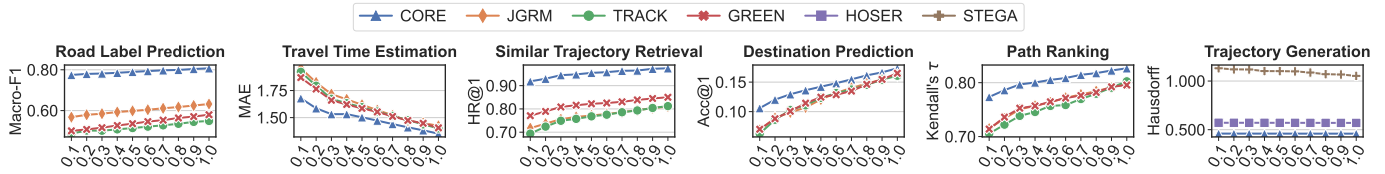


Fig. 18. Results of using varying proportions of training data on the Porto dataset.

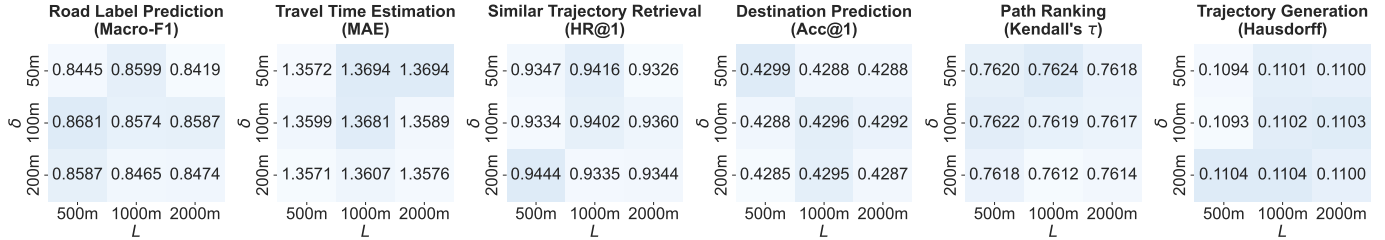


Fig. 19. Sensitivity of CORE to spatial perception scale hyperparameters (δ and L) on the Chengdu dataset.

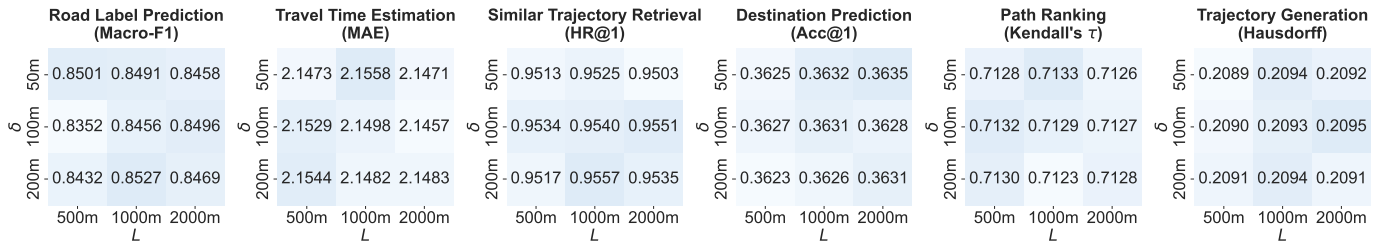


Fig. 20. Sensitivity of CORE to spatial perception scale hyperparameters (δ and L) on the Xi'an dataset.

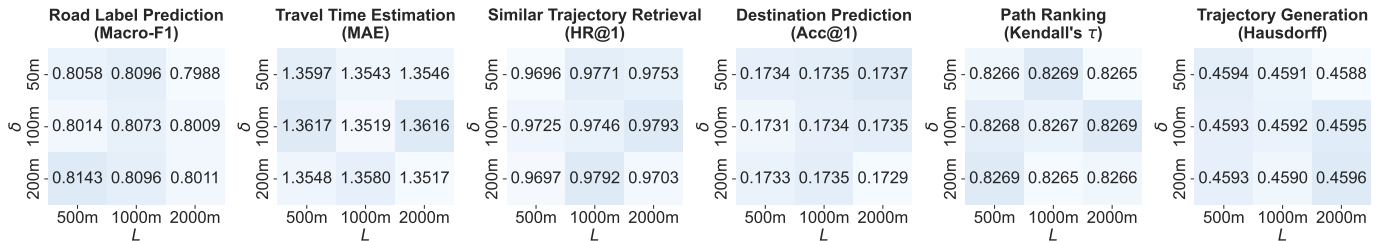


Fig. 21. Sensitivity of CORE to spatial perception scale hyperparameters (δ and L) on the Porto dataset.

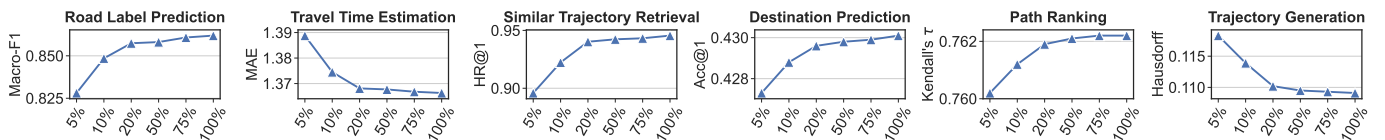


Fig. 22. Impact of the critical segment selection ratio η on the Chengdu dataset.

C. Sensitivity Analyses

1) *Hyperparameter Sensitivity*: Figures 19 to 21 show the sensitivity of CORE to the spatial perception hyperparameters (i.e., the POI perception radius δ and the grid side length L) on the Chengdu, Xi'an, and Porto datasets. Within the examined ranges, performance remains stable, suggesting that CORE does not critically depend on a specific choice of spatial scale.

In addition, Figures 22 to 24 illustrate the impact of the critical segment selection ratio η on the Chengdu, Xi'an, and Porto datasets. The observed trends align with those in the main text, confirming that the top 20% selection strategy consistently offers a favorable trade-off between performance and efficiency across diverse urban environments.

2) *Sensitivity to POI Completeness*: Figures 25 to 27 report the impact of POI completeness on CORE across the Chengdu, Xi'an, and Porto datasets. The observed trends align perfectly with those in the main text, confirming that CORE consistently maintains robustness against sparse environmental data across diverse urban scenarios.

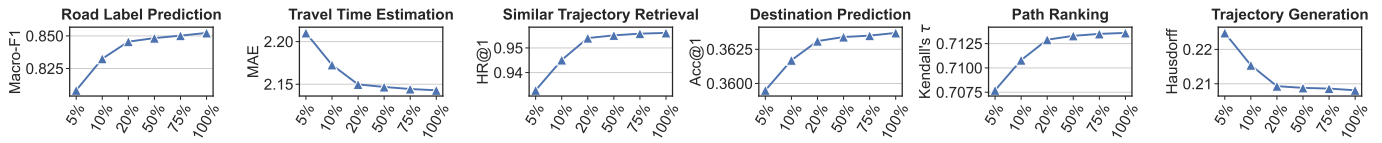


Fig. 23. Impact of the critical segment selection ratio η on the Xi'an dataset.

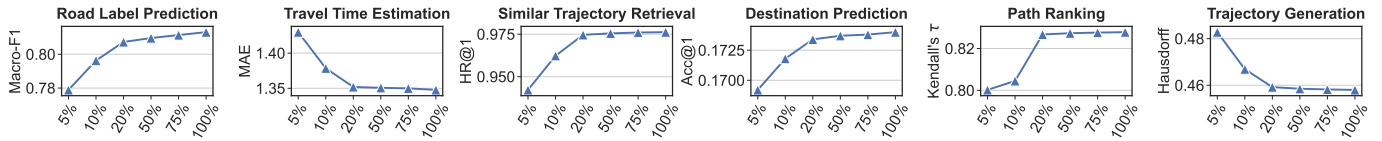


Fig. 24. Impact of the critical segment selection ratio η on the Porto dataset.

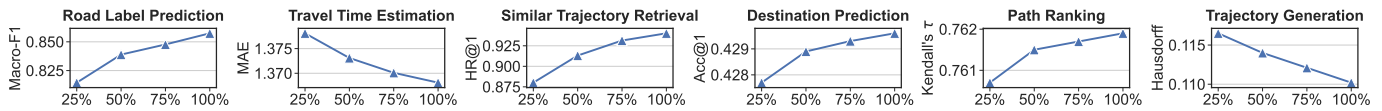


Fig. 25. Sensitivity of CORE to POI completeness on the Chengdu dataset.

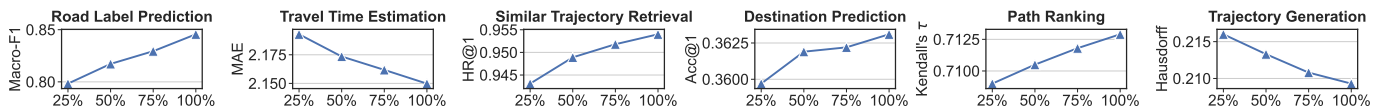


Fig. 26. Sensitivity of CORE to POI completeness on the Xi'an dataset.

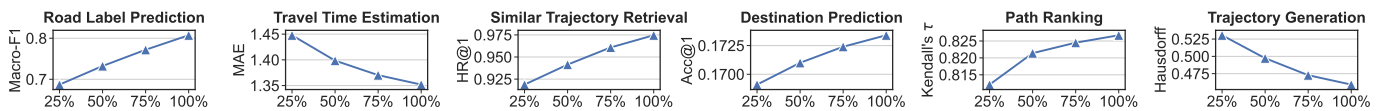


Fig. 27. Sensitivity of CORE to POI completeness on the Porto dataset.